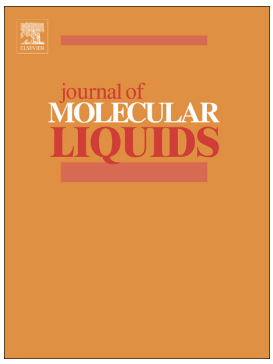

Synthesis, characterization, theoretical calculations and biochemical evaluation of a novel oxime ligand with complexes

Güvenç Görgülü, Bülent Dede

PII: S0167-7322(19)30664-6
DOI: https://doi.org/10.1016/j.molliq.2019.03.169
Reference: MOLLIQ 10710

To appear in: *Journal of Molecular Liquids*

Received date: 3 February 2019
Revised date: 11 March 2019
Accepted date: 29 March 2019

Please cite this article as: G. Görgülü and B. Dede, Synthesis, characterization, theoretical calculations and biochemical evaluation of a novel oxime ligand with complexes, Journal of Molecular Liquids, https://doi.org/10.1016/j.molliq.2019.03.169

Date : 03 Februaty 2019

Author Name : Dr. Bülent DEDE

University : Süleyman Demirel University

Address : Süleyman Demirel University Faculty of Arts & Sciences, Department of Chemistry 32260 Isparta TURKEY

Tel : +90 246 2114153

E-mail : bulentdede@sdu.edu.tr

I am enclosing herewith a manuscript entitled "SYNTHESIS, CHARACTERIZATION, THEORETICAL CALCULATIONS AND BIOCHEMICAL EVALUATION OF A NOVEL OXIME LIGAND WITH COMPLEXES" for possible evaluation in "JOURNAL OF MOLECULAR LIQUIDS". We expect, our findings about molecular docking studies, enzymatic activities and DFT calculations of a novel aminoketooxime ligand and its Mn(II) and Cu(II) complexes are likely to be of great interest to the vision scientists, researchers, and trainees who read your journal. The corresponding author of this manuscript is (Dr. Bülent DEDE) and co-author has been mentioned below according to their contribution.

1. Dr. Güvenç GÖRGÜLÜ

With the submission of this manuscript, I would like to undertake that:

- All authors of this research paper have directly participated in the planning, execution & analysis of this study.
- All the co-authors are aware of and approve of the submission.
- All authors of this paper have read and approved the final version submitted.
- The content of this manuscript have not been copyrighted or published previously.
- The content of this manuscript is not now under consideration for publication elsewhere.
- The content of this manuscript will not be copyrighted, submitted, or published elsewhere, while acceptance by the journal is under consideration.
- There are no directly related manuscripts published or unpublished by any authors of this paper.
- My Institute's (Süleyman Demirel University) representative is fully aware of this submission.

Dr. Bülent DEDE
(Corresponding Author)

Potential Reviewers

1. Dr. Tanurima Bhaumik e-mail: tanurimabhaumik@gmail.com
Department of Chemistry, Jadavpur University, Kolkata, India

2. Dr. Zbigniew Kałuża e-mail: zbigniew.kaluza@icho.edu.pl
Institute of Organic Chemistry Polish Academy of Sciences, Warsaw, Poland

3. Dr. Jan Veselý e-mail: jxvesely@natur.cuni.cz
Department of Organic Chemistry, Charles University, Prague, Czech Republic

SYNTHESIS, CHARACTERIZATION, THEORETICAL CALCULATIONS AND BIOCHEMICAL EVALUATION OF A NOVEL OXIME LIGAND WITH COMPLEXES

Güvenç GÖRGÜLÜ[1], Bülent DEDE[2]*

[1]Mehmet Akif Ersoy University, Faculty of Education, Department of Science Education, Burdur, Turkey

[2]Süleyman Demirel University, Faculty of Sciences and Arts, Department of Chemistry, Isparta, Turkey

*e-mail: bulentdede@sdu.edu.tr

Tel: +90 246 2114153

ABSTRACT

A novel amine containing ketooxime ligand (HBOX) and its Cu(II) and Mn(II) complexes were synthesized, characterized and tested for some of their biological activities. Structural characterization was carried out by elemental analysis, ICP-OES, ^{1}H- and ^{13}C-NMR, UV-Vis, FT-IR, XRD, TG-DTG, magnetic susceptibility and molar conductivity measurements. Elemental analyses, stoichiometric and spectroscopic data of the metal complexes indicated that the metal:ligand ratio was found to be 1:2 and the metal ions were coordinated to the oxime oxygen and amine nitrogen atoms. Furthermore, DFT/B3LYP method with 6-311G(d,p) and LANL2DZ basis sets were used for full optimization of molecular geometries of the ligand and complexes, respectively. The vibrational frequencies, isotropic chemical shifts (^{1}H- and ^{13}C-NMR), electronic transition absorption wavelengths, HOMO and LUMO analyses and molecular electrostatic potential (MEP) properties of the synthesized molecules have been calculated. The results obtained experimentally were confirmed by the theoretical data which are in good agreement. Inhibitory capacity of the HBOX was investigated against neoangiogenic factors, vascular endothelial growth factor receptor-2 (VEGFR-2) and cyclooxygenase-2 (COX-2) by molecular docking studies. HBOX bound to 1CX2 protein with 2 hydrogen bonds at the lowest energy level which indicates the most stabilized form of the protein ligand complex. Complexes were also tested for their catecholase and phenoxazinone synthase-like activities using spectrophotometric procedures. Catecholase and phenoxazinone synthase-like enzyme activities were spectrophotometrically followed by the increase in absorbance at 400 and 433 nm resulted from the oxidation reaction of 3,5-di-*tert*-butylcatechol and 2-aminophenol to 3,5-di-*tert*-butylquinone and 2-aminophenoxazine-3-one, respectively. According to the calculated k_{obs} values, the Mn(II) complex was found to be more active for both enzymes compared to Cu(II).

Keywords: Oxime, metal complexes, DFT, molecular docking, catecholase-like activity, phenoxazinone synthase-like activity

1. INTRODUCTION

The stability and function of a metal complex basically depend on its design and synthesis, besides, the electronic configuration of added metal ion(s) and electron delocalization of added functional groups. Since the existence of an oxime group in the ligand increase stability, strength and biological activity of the complex, they used extensively in industry, medicine and environmental protection [1]. Illuminating the structures of these ligands and metal complexes, therefore, become important to understand their functioning related to configuration [2]. Besides spectroscopic and analytical techniques, DFT gives valuable information on structural, energetic, molecular, electronic, vibrational and magnetic behaviour which makes an important contribution for the characterization of the interested compound [3].

In addition to their antioxidant, antibacterial, antifungal and antiviral properties, oxime compounds are also used as potential agents for the inhibition of tumour growth [4-11]. It is still critically important to inhibit molecules increasing in pathological conditions like chronic inflammation, tumour growth and metastasis [12]. Pathological angiogenesis plays a key role in tumour growth and metastasis with a cascade mechanism [13]. Vascular endothelial growth factor-2 (VEGFR-2) is often used as a parameter for being a potent metastatic factor due to its angiogenic and lymphangiogenic effects [14]. It also promotes the angiogenic process by inducing cyclooxygenase (COX-2) and inducible nitric oxide synthase (iNOS) [15,16].

Molecular docking research focuses on computationally simulating the molecular recognition process. It aims to achieve an optimized conformation with the best orientation between the target protein and ligand such that the free energy of the overall system is

minimized [17]. The application of docking in a targeted drug-delivery system is a huge benefit. One can study the size, shape, charge distribution, polarity, hydrogen bonding, and hydrophobic interactions of both the ligand (prospective drug) and the receptor (target site) [18].

It is not possible to use natural enzymes as drugs due to their instability in solution and delivery problems, while metal complexes are better candidates so far for medical uses [19-22]. Oxime containing complexes have the potential use as the catalysts due to their natural enzyme mimicking abilities [23-26]. Oxidoreductase family of enzymes involves in various life-sustaining reactions ranging from the simplest organism to human beings. Catecholase (catechol oxidase: EC 1.10.3.1) and phenoxazinone synthase (*o*-aminophenol oxidase: EC 1.10.3.4) are the members of this group both carrying a Cu(II) atom in their active site as a cofactor which is one of the factors we considered during the design of the complexes [27].

In this study, an oxime containing ligand (HBOX: Hydrogen Biphenyl OXime) and its mononuclear Cu(II) and Mn(II) complexes were synthesized and characterized spectrophotometrically and theoretically. The structural and spectroscopic data of the HBOX and its metal complexes in the ground state were calculated by using DFT/B3LYP/6-311G(d,p) and DFT/B3LYP/LANL2DZ levels, respectively. Molecular docking studies were performed to understand the antiangiogenic efficiency of the HBOX ligand. In addition, enzymatic potentials of both complexes were tested for catecholase and phenoxazinone synthase-like activities.

2. EXPERIMENTAL

2.1. Physical Measurements

All chemicals acquired commercially in their highest purity grade were used as they received. The instruments used in our experiments were as follows: ^{1}H- and ^{13}C-NMR spectra of the ligand were recorded on a JEOL NMR-400 MHz spectrometer, using TMS as an internal standard and chloroform as a solvent. Spectrophotometric measurements were applied with a PG T80+ UV-Vis spectrometer. FT-IR spectra of the synthesized ligand and its metal complexes were measured using a Schimadzu IRPrestige-21 FT-IR spectrophotometer within the range 4000-400 cm^{-1}, using KBr disc pellets. Powder X-ray diffraction (XRD) pattern of the complex was recorded with a Bruker AXS D8 Advance X-ray diffractometer. In addition, LECO 932 CHNS analyzer was used to determine C, H and N proportion of the compounds. Perkin Elmer Optima 5300 DV ICP-OES spectrometer was used to obtain metal contents of the complexes. Also, molar conductance of the complexes in DMF (10^{-3} M solution) were measured on an Optic Ivymen System conductivity meter at room temperature. Melting points were determined with an Electrothermal model IA 9100 digital instrument. Magnetic moment value measurements were carried out at room temperature on a Sherwood Scientific Magnetic Susceptibility Balance (Model MX1).

2.2. Synthesis of Ligand [*2-([1,1'-biphenyl]-4-yl)-N-(3,4-dimethylphenyl)-N'-hydroxy-2-oxoacetimidamide (HBOX)*]

1-(biphenyl-4-yl)ethanone and 2-(biphenyl-4-yl)-2-oxoacetaldehyde oxime was synthesized according to the literature [28-30]. As a starting material, 2 mmol, 0.519 g of 2-(biphenyl-4-yl)-N-hydroxy-2-oxoacetimidoyl chloride was dissolved in 20 mL EtOH. The mixture was

cooled and kept at -5°C during dropwise addition of ethanol solution of 4 mmol 3,4-dimethyl aniline to the solution of chloroketooxime over 15 min. Expected precipitation and color change were observed in the reaction medium just after the addition. The reaction mixture left stirring 2 hours at minus temperatures. Then it was allowed to stir at ambient temperature at least for 2 more hours. The resulting precipitation was filtered, washed by aqueous sodium bicarbonate (1% w/v), distilled water and ethanol and then, dried on P_2O_5.

2.2. Synthesis of Complexes [*Cu(BOX)$_2$H$_2$O and Mn(BOX)$_2$H$_2$O*]

For the synthesis of the complexes, 0.30 mmol $Cu(CH_3COO)_2.H_2O$ (0.029 g) or $Mn(CH_3COO)_2.4H_2O$ (0.036 g) in 30 mL ethanol was added to previously prepared 30 mL ethanol solution of the ligand HBOX. After stirring in water bath at 40^{o}C for a few minutes, the pH was adjusted to 5.5-6 with KOH solution containing 1% of ethanol. Stirring continued for 2 more hours and the mixture transferred to +4^{o}C after cooling and kept overnight. Final solution was filtered, the precipitation was rinsed with water and ethanol and left to dry.

2.3. Theoretical Calculations

Theoretical calculations were carried out by the Gaussian 09 software [31] with the DFT level of theory. Optimizations and frequency calculations were performed by B3LYP functionals with 6-311G(d,p) and LANL2DZ basis set [32,33] in the gas phase. Files obtained from the optimization were introduced as the starting file for succeeding calculations. For graphics and other simulations, GaussView 5.0.9 program was used [34]. Uv-Vis spectrums and electronic properties like HOMO and LUMO energies were obtained by TD-DFT method with the same set. Molecular orbital contributions were calculated by GaussSum program [35]. Finally, the ^{1}H- and ^{13}C-NMR data were calculated by GIAO method [36,37].

2.4. Molecular Docking

Molecular docking studies were performed on SwissDock web server using EADock DSS algorithm [38]. High resolution crystal structures of VEGFR-2 (PDB ID: 2XIR) and COX-2 (PDB ID:1CX2) were obtained from protein data bank (https://www.rcsb.org). COX-2 subunit A was used for simplicity and a better display among the four subunits for docking and visualizing. All images in molecular docking studies were drawn with the UCSF Chimera package [39].

2.5. Enzymatic Activity Studies

2.5.1. Catecholase-Like Enzyme Activity

Catecholase-like activity of the complexes were measured by the enzymatic conversion of substrate 3,5-di-*tert*-butylcatechol (3,5-DTBC, $5x10^{-3}$ M) to quinone product 3,5-di-*tert*-butyl-*o*-benzoquinone (3,5-DTBQ) by Cu(II) and Mn(II) complexes ($1x10^{-4}$ M each). The increase in product was followed spectrophotometrically by the increase in absorbance at 400 nm with 30 sec. intervals. The method was modified from Reim and Krebs [40].

2.5.2. Phenoxazinone Synthase-Like Enzyme Activity

Cu(II) and Mn(II) complexes were tested for phenoxazinone-like activity. For the reaction to occur, $1.67x10^{-4}$ M of complex as the enzyme with $12.5x10^{-3}$ M 2-aminophenol (OAPH) as the substrate were mixed and final volume was adjusted to 25 mL with DMF. The formation of 2-aminophenoxazine-3-one (APX) as the product was followed spectrophotometrically by the increase in absorbance at 433 nm with 30 sec. intervals [41]. The rate constants (k_{obs}) for both enzymatic reactions, catalysed by both complexes were calculated from the equation below.

$$\ln(A_\infty/A_\infty - A_t) = kt$$

A_∞ and A_t are the absorbances of the formed product at time = ∞ and time = t

3. RESULTS AND DISCUSSION

The route for the synthesis of the HBOX ligand is shown in Fig. 1. Numerous physical and spectroscopic methods have been used for the characterization of compounds. Measured and calculated physical properties of the compounds are given in Table 1.

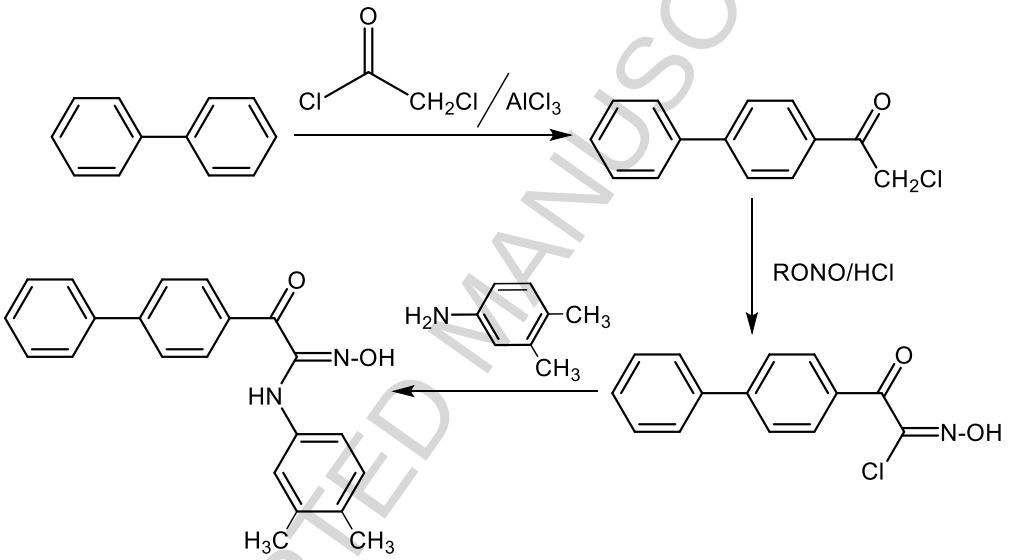

Figure 1. Synthetic plan for the 2-([1,1'-biphenyl]-4-yl)-N-(3,4-dimethylphenyl)-N'-hydroxy-2-oxoacetimidamide ligand (HBOX)

Table 1. Some physical data and elemental analysis results of the synthesized compounds

Compound	μ_{eff} (B.M.)	Conductivity ($\Omega^{-1}cm^2mol^{-1}$)	Color Yield (%)	Melting Point (^oC)	Found (Calculated) %			
					C	H	N	Metal
HBOX	-	-	Bright yellow (81)	178	76.58 (76.72)	5.73 (5.85)	8.34 (8.13)	-
$Cu(BOX)_2H_2O$	1.78	9.5	Dark brown (59)	280	68.96 (68.78)	5.48 (5.25)	7.06 (7.29)	8.52 (8.27)
$Mn(BOX)_2H_2O$	5.94	6.7	Black (44)	>300	69.28 (69.56)	5.56 (5.31)	7.14 (7.37)	7.47 (7.23)

3.1. ^{1}H- and ^{13}C-NMR spectra

^{1}H- and ^{13}C-NMR spectra were recorded in chloroform and calculated by the use of gauge-including atomic orbital (GIAO) method (Fig. S1 and S2) and both chemical shift data are shown in Table 2 and 3. The ^{1}H-NMR spectrum of the HBOX showed a D_2O exchangeable proton (H35) at 8.14 ppm due to the oxime group. This chemical shift value in the lowest field of the spectrum was calculated as 8.65 ppm. The C-H protons of the aromatic groups were recorded in 6.56-7.69 ppm range as multiplet peaks. These values were calculated between 6.47-8.55 ppm. The chemical shift for the N-H proton of the amine group in the HBOX was appeared at 5.92 ppm. The H40 proton, bound to the highly electronegative nitrogen atom, was calculated in a slightly lower area than the experimental result (calc. 6.27 ppm). Since the nitrogen was adjacent to the aromatic ring, this shift might be affected by the structures in resonance. Additionally, signals observed at the 2.13 and 1.59 ppm were attributable to the H41-H46 protons of the HBOX. Their corresponding calculated chemical shift appeared at 2.37 and 1.98 ppm, respectively.

Table 2. Recorded and calculated chemical shift values of the HBOX in ^{1}H-NMR spectra

δ(ppm)

Atom	Experimental (in $CDCl_3$)	Theoretical (in $CDCl_3$)
H41-H46 (aliphatic)	1.59 (s, 3H) 2.13 (s, 3H)	1.98 2.37
H40 (amine)	5.92 (s, 1H)	6.27
H27-H34 H36, H37-H39 (aromatic)	6.56-7.69 (m, 12H)	6.47-8.55
H35 (oxime)	8.14 (s, 1H)	8.65

s:singlet, m:multiplet

By considering the ^{13}C-NMR spectra of the HBOX molecule, the peak observed at 186.58 ppm was assigned to the carbonyl carbon (C13) which was calculated as 170.41 ppm at the mentioned level of theory. The signal at 149.24 ppm assigned to the C14 carbon of the oxime group was computed as 135.06 ppm. The oxime carbon was also observed in a low region such as carbonyl carbon. High electronegative nitrogen and oxygen atoms adjacent to the oxime carbon caused such a downfield shift. The chemical shifts for the aromatic ring carbons (C1-C12 and C19-C24) were appeared in the range of 118.29-146.66 ppm and the calculated range for these carbons was between 102.20-134.80 ppm. The highly shielded methyl carbons (C25, C26) of the HBOX molecule showed signals at 19.18 and 19.98 ppm and calculated as 11.23 and 11.97 ppm, respectively. Comparison of experimental and theoretical ^{1}H- and ^{13}C-NMR spectra revealed that, the chemical shifts were found to be compatible with each other and in good agreement with the data reported in the other oxime molecule researches [42-48]. The theoretical chemical shifts seem to appear in lower region approximately 15 ppm compared to the experimental shifts for ^{13}C-NMR.

Table 3. Recorded and calculated **c**hemical shift values of the HBOX in ^{13}C-NMR spectra

δ(ppm)

Atom	Experimental (in $CDCl_3$)	Theoretical (in $CDCl_3$)
C25, C26 (aliphatic)	19.18, 19.98	11.23, 11.97
C1-C12, C19-C24 (aromatic)	118.29-146.66	102.20-134.80
C14 (oxime)	149.24	135.06
C13 (carbonyl)	186.58	170.41

3.2. FT-IR spectra

The calculated vibrational wavenumbers were scaled as 1.0119 for frequencies lower than 1800 cm^{-1} and 0.9682 for frequencies higher than 1800 cm^{-1} [49]. Some experimental and calculated wavenumbers for the HBOX and its mononuclear Cu(II) and Mn(II) complexes are given in Table 4. Comparative experimental and calculated spectra are also given for HBOX, $Cu(BOX)_2H_2O$ and $Mn(BOX)_2H_2O$ in Fig. S3, S5 and S6, respectively. FT-IR spectra of the HBOX showed a broad band at 3231 cm^{-1} which was assigned to (O-H) stretching vibration of oxime group. The theoretical frequency of this band was found to be as 3126 cm^{-1}. This band was disappeared with the formation of the complex and new bands were appeared at 3645 cm^{-1} (calc. 3716) and 3638 cm^{-1} (calc. 3702) for the $Cu(BOX)_2H_2O$ and $Mn(BOX)_2H_2O$, respectively. The disappearance of the band belonging to the O-H of oxime group showed that the HBOX ligand participated to the coordination via the oxime oxygen atom. The broad bands around 3600 cm^{-1} can be assigned to the coordination water in the complexes. Since the theoretical calculations were done in gaseous phase, the calculated frequencies for the coordination water deviated about 70 cm^{-1}. The peak observed at 3382 cm^{-1} was assigned to the ν(N-H) and its computed wavenumber was found as 3451 cm^{-1}. The band at 3382 cm^{-1} underwent a shift to lower frequencies about 60 cm^{-1} by the complexation which indicates the

coordination of the nitrogen atom of amine with metal ions. Coordination of the oxime oxygen and the amine nitrogen atoms in the complexes was proved by the appearance of new bands at about 545 and 450 cm^{-1}, which were assigned to ν(M-O) and ν(M-N), respectively [50,51]. Theoretically computed M-O and M-N stretching vibrations were appeared at about 580 and 470 cm^{-1}, respectively.

Table 4. Some selected band frequencies (cm^{-1}) of the HBOX and its Cu(II) and Mn(II) complexes

Compounds		**O-H$_{(water)}$**	**O-H$_{(oxime)}$**	**N-H**	**C=N**	**N-O**	**C-N**	**M-O**	**M-N**
HBOX	Exp.	-	3231b	3382m	1602s	1384s	1510s	-	-
	Theo.	-	3126	3451	1628	1387	1524	-	-
Cu(BOX)$_2$H$_2$O	Exp.	3645b	-	3323b	1599s	1453m	1503s	547w	445w
	Theo.	3716	-	3364	1611	1458	1518	582	471
Mn(BOX)$_2$H$_2$O	Exp.	3638b	-	3327b	1598s	1452m	1492m	545w	449w
	Theo.	3702	-	3371	1612	1464	1513	577	475

b:broad, s:sharp, m:medium, w:weak

The C=N vibration of oxime group of the HBOX was observed as a sharp band at 1602 cm^{-1}. The same vibration appeared at 1628 cm^{-1} in theoretical spectrum. Since the oxime nitrogen was not directly involved in coordination, no significant shift was observed in the stretching vibration of this band with complexation. However, the stretching vibration at 1384 cm^{-1}, belonging to the N-O bond of the ligand oxime, shifted to 1453 cm^{-1} (calc. 1458) for $Cu(BOX)_2H_2O$ and 1452 cm^{-1} (calc. 1464) for $Mn(BOX)_2H_2O$ with the complex formation. These shifts to higher wavenumbers also supported that the ligand was participated in

coordination through the oxygen atom of the oxime group [42]. Data obtained from the FT-IR spectra showed that the experimental frequencies were quite compatible with the theoretical ones.

3.3. Uv-vis spectra and Frontier Molecular Orbital Analysis

Uv-vis spectra of the HBOX and its mononuclear Cu(II) and Mn(II) complexes were recorded in ethanol solvent. Electronic parameters such as the oscillator strengths, excitation energies and absorption wavelengths were calculated using TD-B3LYP/6-311G(d,p) level of theory in same solvent. Experimentally obtained and computed Uv-vis spectra of the HBOX are shown in Fig. S4 using the same scale and electronic parameters are also given in Table 5 and 6. The experimental Uv-vis absorption spectrum of the free HBOX ligand showed three maximum wavelength values at 295, 316 and 339 nm. The band at 295 nm was due to $\pi \rightarrow \pi^*$ transitions in the benzene ring [52]. Its corresponding calculated wavelength as the most intense band was observed at 318 nm (f=0.5822) with HOMO-1→LUMO (76%) and HOMO-6→LUMO (20%) contributions. No shifting at 295 cm^{-1} band by the complex formation indicated that the benzene ring was not participated in the coordination.

Table 5. Electronic transitions, wavelengths, oscillator strengths and major contributions for HBOX in ethanol solvent

Transitions	Experimental		Theoretical B3LYP/6-311G(d,p)			
	λ (nm)	E (eV)	λ (nm)	E (eV)	f	Major contributions
$\pi \rightarrow \pi^*$ (benzene)	295	4.20	318	3.90	0.5822	H-1→L (76%) H-6→L (20%)
$\pi \rightarrow \pi^*$ (imine)	316	3.92	332	3.73	0.1149	H-6→L (65%), H-1→L (21%)
$n \rightarrow \pi^*$	339	3.66	434	2.86	0.0198	H→L (99%)

The band at 316 nm can be attributed to π→π* transitions of the imine moiety of oxime group (calc. 332 nm). The band calculated at 332 nm was composed of the HOMO-6→LUMO and HOMO-1→LUMO with 65% and 21% contributions, respectively. The imine group was also affected by the binding of oxime oxygen to the metal ions, which was shifted to the lower wavelengths for $Cu(BOX)_2H_2O$ complex (300 nm) and to higher wavelengths for the $Mn(BOX)_2H_2O$ complex (328 nm). The band appeared at 339 nm was attributed to the $n \rightarrow \pi^*$ transitions of the free ligand and its corresponding wavelength was calculated as 434 cm^{-1} which was occurred between HOMO and LUMO with 99% contribution. The band at 339 nm corresponding to the n→π* transitions of the HBOX was observed at 310 and 360 nm in the $Cu(BOX)_2H_2O$ and $Mn(BOX)_2H_2O$ spectra, respectively. These shifts were indicated that the ligand was coordinated through the oxime oxygen. The weak bands observed at 504 and 695 nm in the spectra of the complexes, which can't be seen in the spectrum of HBOX, were originated from the d→d transitions of the metal ions [52]. These transitions revealed that both $Cu(BOX)_2H_2O$ and $Mn(BOX)_2H_2O$ complexes were in distorted square-pyramidal geometry [53].

Table 6. Electronic transitions and wavelengths of metal complexes of the HBOX in ethanol solvent

Complexes	$\pi \rightarrow \pi^*_{(benzene)}$	$\pi \rightarrow \pi^*_{(imine)}$	$n \rightarrow \pi^*$	$d \rightarrow d$
$Cu(BOX)_2H_2O$	295	300	310	504
$Mn(BOX)_2H_2O$	295	328	360	695

It is well known that the energy gap between the highest occupied molecular orbital (HOMO) and the lowest unoccupied molecular orbital (LUMO) gives valuable information about the chemical reactivity, stability and polarizability of the molecules [54,55]. 3D plot with energy gap value between HOMO and LUMO of HBOX and its Cu(II) and Mn(II) complexes are given in Fig. 2-4. Calculated energy gap value for the HBOX between the ground state and the first exited state was found to be 3.504 eV. This calculated energy gap was smaller than the conventional oxime bearing compounds in the literature [56,57]. The lower the energy gap corresponds to the higher the reactivity of the HBOX molecule. As can be seen from Fig 2., the majority of HOMO was localized on dimethlybenzene moiety whereas the LUMO was mainly on the biphenyl region.

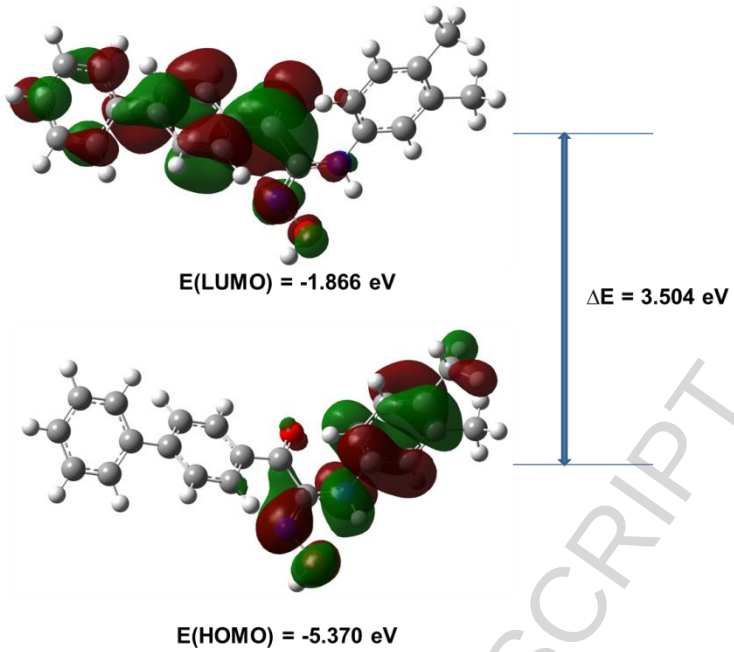

Figure 2. Molecular orbital surface and HOMO-LUMO gap of the HBOX computed at B3LYP/6-311G(d,p) level

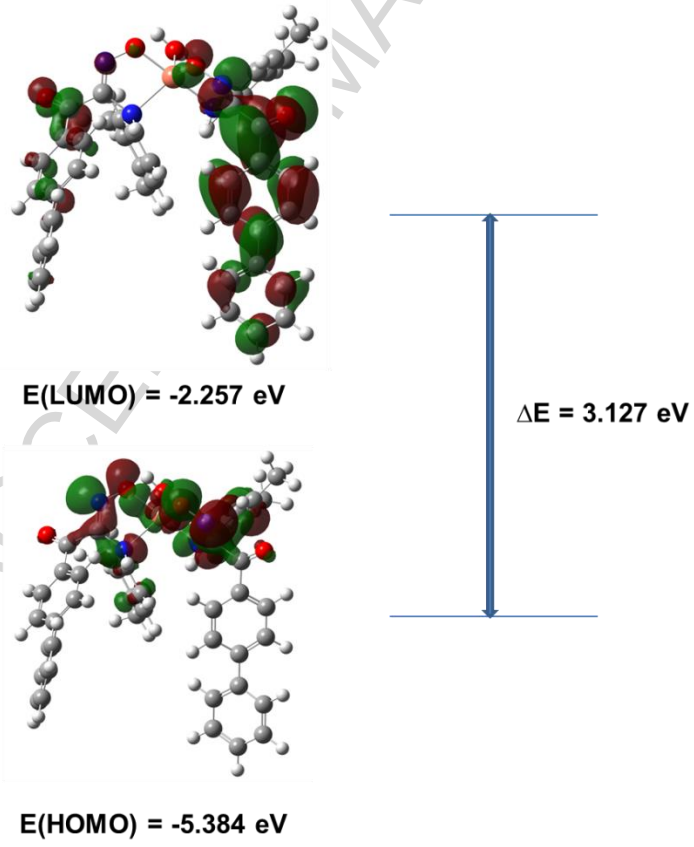

Figure 3. Molecular orbital surface and HOMO-LUMO gap of the $Cu(BOX)_2H_2O$ computed at B3LYP/LANL2DZ level

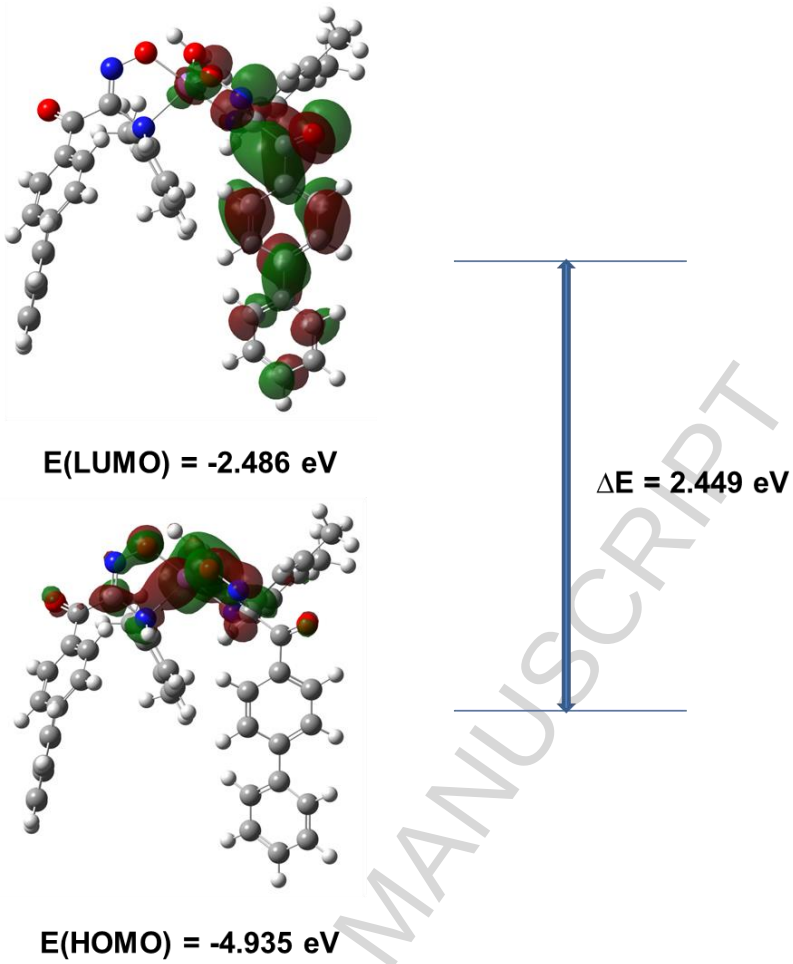

Figure 4. Molecular orbital surface and HOMO-LUMO gap of the $Mn(BOX)_2H_2O$ computed at B3LYP/LANL2DZ level

3.4. Thermal Analysis

The thermogravimetry (TG) curves give information on the thermal stability and the products formed on heating. Thermal analyses for the HBOX and its metal complexes were performed within the temperature range from ambient temperature up to 1000^{o}C. In TG, the changes in the weight of the molecule were recorded as a function of the temperature during heating. The TG curve was also supported by the derivative thermogravimetry (DTG) curves.

The thermal behaviour of both complexes was almost the same. For this reason, only $Cu(BOX)_2H_2O$ complex were discussed here in detail. The thermogram of the HBOX and

$[Cu(BOX)_2H_2O]$ are shown in Fig 5 and 6, respectively. The critical data obtained from the investigation of the thermograms are given in Table 7.

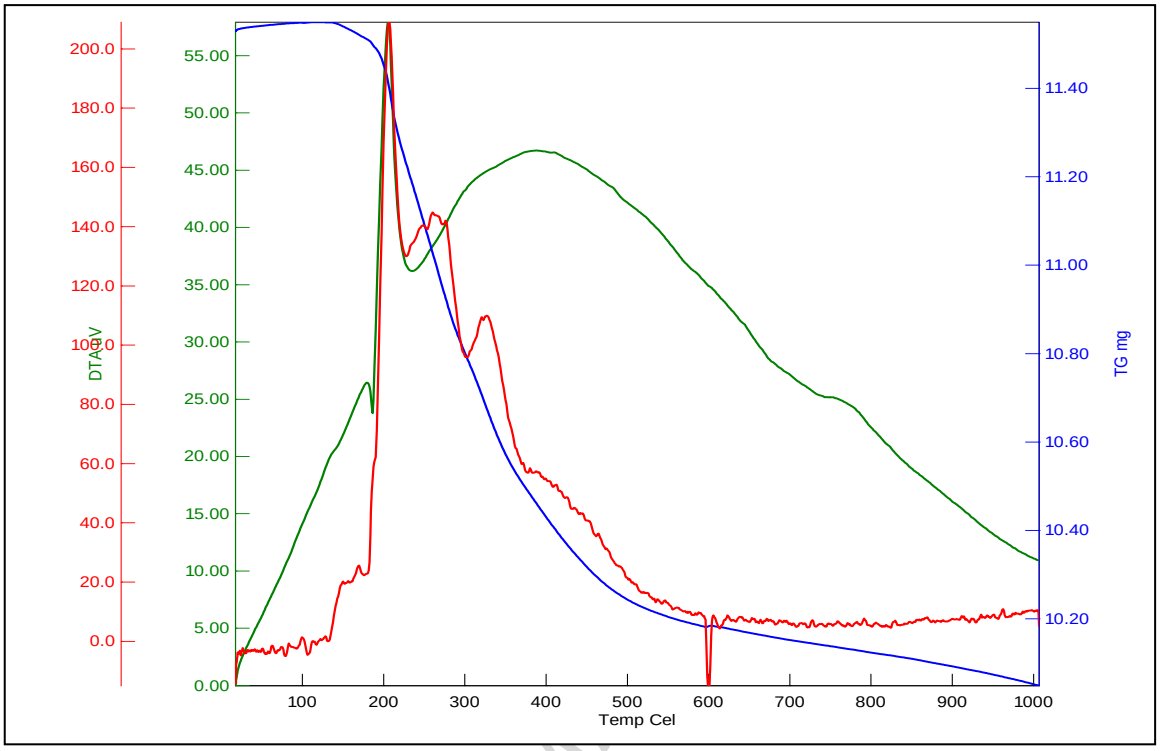

Figure 5. Thermogram of the HBOX taken between room temperature and 1000°C

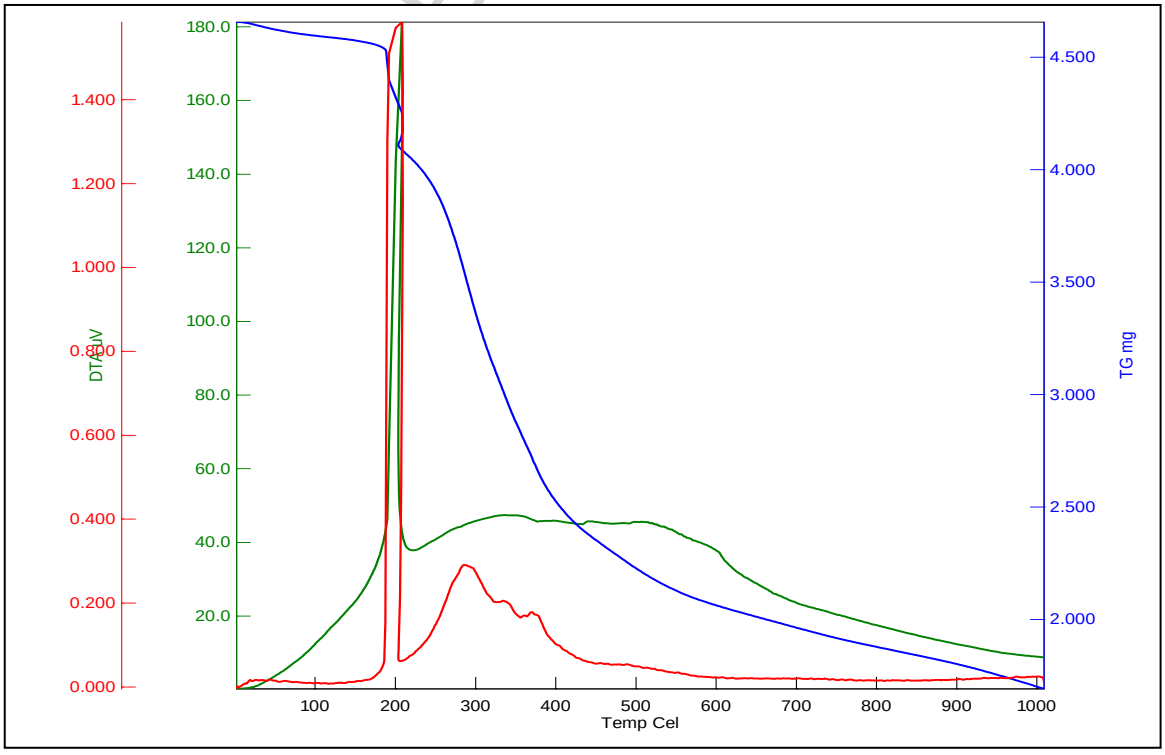

Figure 6. Thermogram of the $[Cu(BOX)_2H_2O]$ taken between room temperature and 1000°C

The HBOX ligand with the molecular formula $C_{22}H_{20}N_2O_2$ was thermally decomposed in two successive degradation steps. The first step occurs between 170 and 510^{o}C with a mass loss of 9.21% (calc. 9.29%) which is reasonably accounted for the loss of 1 mole of hydroxyl and 1 mole of methyl groups. The second degradation step started at 510^{o}C but the decomposition was not completed at 1000^{o}C.

The thermal decomposition of the $[Cu(BOX)_2H_2O]$ with the molecular formula $[C_{44}H_{40}CuN_4O_5]$ was taken place in four succeeding stages. In the first stage, from 20 to 195^{o}C, one mole of coordinated H_2O molecule degraded with a 2.32% mass loss (calc. 2.34%). The second stage started at 195^{o}C and ended at 215^{o}C in which the corresponding mass loss of 11.72% was due to the degradation of 2 moles of oxime groups confirming the calculated value (calc. 10.93%). The DTG curve showed a peak at 215^{o}C for this stage. The third estimated mass loss of 39.52% (calculated mass loss, 39.82%), occurred within the temperature range of 215-550^{o}C, can be attributed to the liberation of 2 moles of biphenyl groups. In the DTG curve, three peaks at 290, 350 and 380^{o}C were observed for this region. The last decomposition stage started at 550^{o}C was still in progress at 1000^{o}C. By considering the thermal analyses results, found and calculated mass loss percentages obtained from the related decomposition stages were in good agreement.

Table 7. Thermoanalytical results (TG, DTG) of the HBOX and $Cu(BOX)_2H_2O$

Compounds	TG range (^oC)	DTGmax (^oC)	Estimated (calculated) %		Assignment	Residue
			Mass loss	Total mass loss		
HBOX	170-510	180, 210, 260, 340	9.21 (9.29)		1 mole of hydroxyl group 1 mole of methyl group	
	510-					Decomposition is in progress
$Cu(BOX)_2H_2O$	20-195	-	2.32 (2.34)		1 mole of coordinated water	
	195-215	215	11.72 (10.93)		2 mole of oxime groups	
	215-550	290, 350, 380	39.52 (39.82)		2 mole of biphenyl groups	
	550-					Decomposition is in progress

3.5. X-ray Diffraction

X-ray diffraction measurement was carried out to obtain further evidence of the structure of the $Mn(BOX)_2H_2O$. X-ray pattern of the title complex was recorded at 2θ = 10-90^o range and shown in Fig. 7. It was found that the $Mn(BOX)_2H_2O$ complex showed sharp peaks. The XRD patterns indicated the crystalline nature of the studied complex and this behaviour is due to the incorporation of water molecules into the coordination sphere [58,59]. Attempts to prepare the single crystal synthesis of the both complexes were unsuccessful.

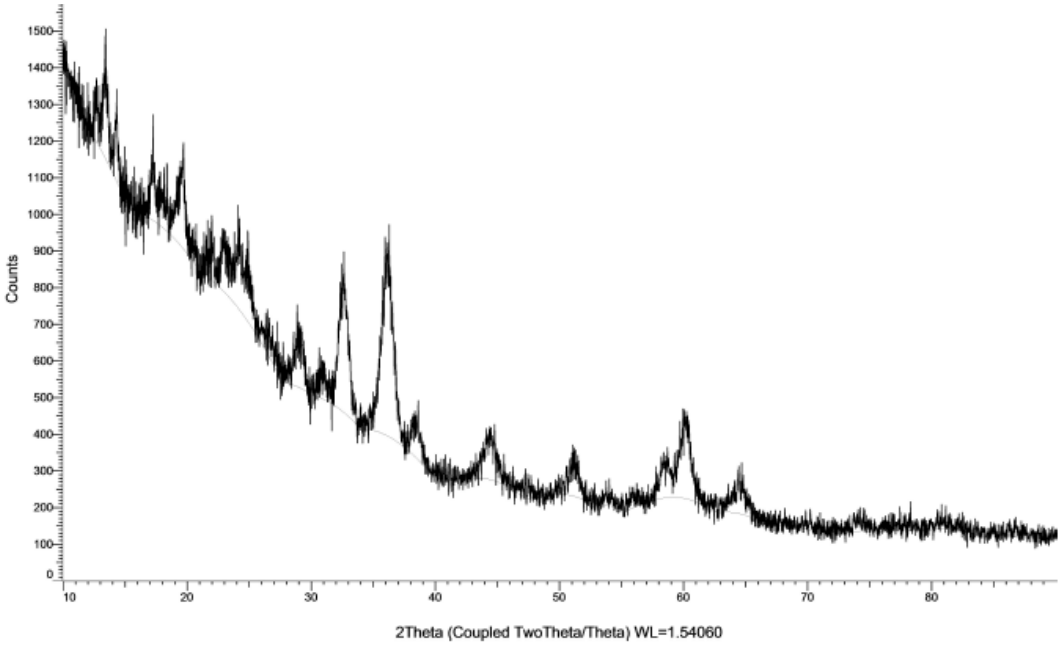

Figure 7. XRD diffraction pattern of the $Mn(BOX)_2H_2O$ complex

Magnetic Susceptibility

The magnetic susceptibilities of the $[Cu(BOX)_2H_2O]$ and $[Mn(BOX)_2H_2O]$ were measured at room temperature using Gouy method and the results were given in Table 1. The results revealed that both complexes were paramagnetic at ambient temperature. Magnetic moment values of the mononuclear complexes were 1.78 and 5.94 B.M. for $[Cu(BOX)_2H_2O]$ and $[Mn(BOX)_2H_2O]$, respectively. By considering the $[Cu(BOX)_2H_2O]$ complex, Cu(II) ion ($3d^9$) had one unpaired electron in its 3d shell, therefore its compounds were considered to have magnetic moments close to the spin-only value of 1.73 B.M. According to the magnetic moment value of $[Cu(BOX)_2H_2O]$, the environment around the Cu(II) was square-pyramidal geometry [60].

On the other hand, the magnetic moment value of [Mn(BOX)2H2O] was close to 5,92 B.M. of high-spin penta-coordinated manganese(II) ion with d^5 electron configuration. It can be concluded from these data that the metal(II) ion in the complexes were coordinated with the

oxime and amine groups in the HBOX and completed five-coordinated geometry with one mole of coordination water.

3.6. Molar Conductivity

The investigation of the molar conductivity values of the complexes was highly supportive of their structures. Molar conductivity measurements were performed in N,N-dimethylformamide solutions at room temperature. Obtained conductivity values for the $[Cu(BOX)_2H_2O]$ and $[Mn(BOX)_2H_2O]$ were found to be 9.5 and 6.7 $\Omega^{-1}cm^2mol^{-1}$, respectively. The molar conductance of the synthesized Cu(II) and Mn(II) complexes in DMF revealed that the complexes had a non-electrolyte nature [61].

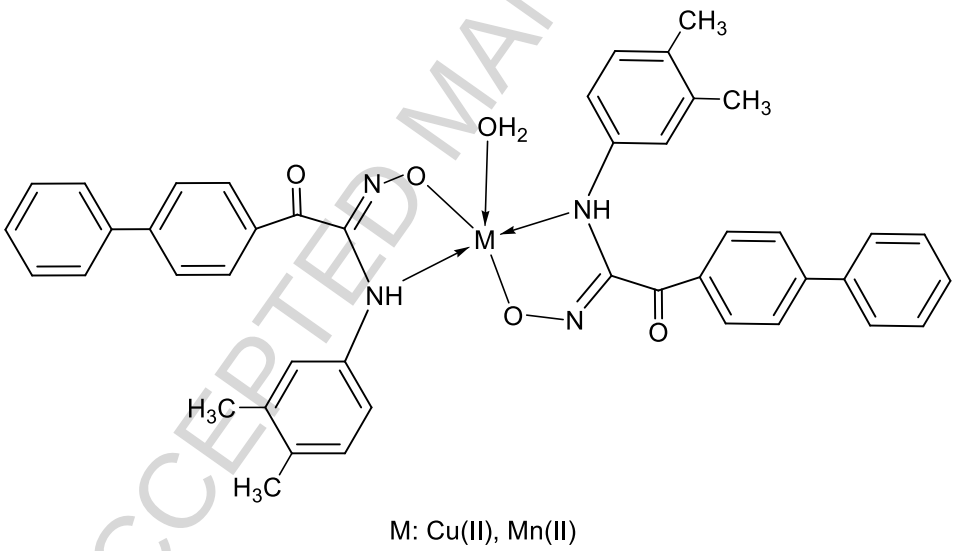

Figure 8. The proposed structure of synthesized complexes

3.7. Computational Details

3.7.1. Molecular Structure

The optimized molecular structure of the HBOX and its mononuclear Cu(II) and Mn(II) complexes were calculated by using B3LYP/6-311G(d,p) and B3LYP/LANL2DZ level of theory, respectively. The numbering schemes of the compounds are given in Fig. 9-11. The optimized parameters (band lengths, bond angles and dihedral angles) of the HBOX and metal complexes calculated by mentioned levels are listed in Table 8 and 9, respectively. The calculated C4-C7 bond length between two benzo rings in biphenyl moiety was found as 1.484 Å. The C10-C13 and C13-C14 bond lengths between biphenyl-carbonyl and carbonyl-oxime groups were computed as 1.489 and 1.518 Å, respectively. In addition, the C14-N15 and N15-O17 bond lengths in the oxime group were found to be 1.299 and 1.419 Å, respectively. When the calculated bond length values of the HBOX molecule were examined collectively it was found that the aliphatic C-C bonds were longer than the aromatic ones and the aromatic ones were longer from the double bonds as expected. The HBOX molecule can be divided into four parts: biphenyl, carbonyl, oxime and amine. The dihedral angles for the C11-C10-C13-C14, O16-C13-C14-N15 and N15-C14-N18-H40 related biphenyl-carbonyl, carbonyl-oxime and oxime-amine moieties were calculated as -167.1^{o}, -134.7^{o} and 8.6^{o}, respectively. This result revealed that the molecular geometry of the HBOX was nonplanar and four parts of the title molecule were not in the same plane.

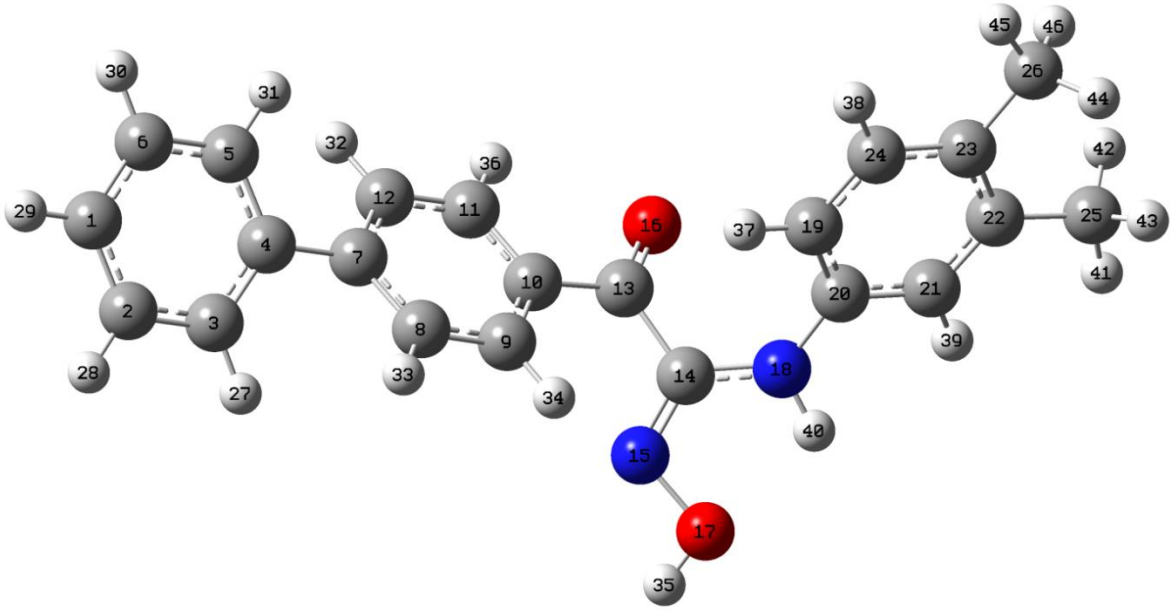

Figure 9. The optimized geometric structure of the HBOX computed at B3LYP/6-311G(d,p) level

C5-C4-C7-C8 dihedral angle was obtained as 143.1^{o} in mentioned level which was revealed that the two benzo rings in biphenyl group was not in same plane, too.

Table 8. Some selected calculated bond lengths (Å), bond and dihedral angles (^{o}) for the HBOX computed at B3LYP/6-311G(d,p) level

Parameters	**B3LYP/6-311G(d,p)**
Bond lengths (Å)	
C5-C6	1.394
C2-C3	1.394
C1-H9	1.086
C4-C7	1.484
C8-C9	1.391
C11-C12	1.387
C11-H36	1.085
C10-C13	1.489
C13-O16	1.222
C13-C14	1.518

C14-N15	1.299
N15-O17	1.419
O17-H35	0.966
C14-N18	1.368
N18-C20	1.410
C19-C24	1.393
C21-C22	1.395
C23-C26	1.510
C22-C25	1.510
C26-H46	1.098
Bond angles (^{o})	
C6-C1-C2	119.5
C5-C4-C3	118.2
C3-C4-C7	120.9
C8-C7-C12	118.0
C9-C10-C11	118.7
C11-C10-C13	117.4
C10-C13-O16	121.8
C14-N15-O17	109.8
C14-N18-C20	129.2
C19-C20-C21	118.9
C20-C19-C24	119.4
C22-C23-C26	121.2
Dihedral angles (^{o})	
C1-C6-C5-C4	-0.1
C5-C4-C7-C8	143.1
C11-C10-C13-C14	-167.1
O16-C13-C14-N15	-134.7
C14-N15-O17-H35	-174.2
C14-N18-C20-C21	-157.9
C10-C13-C14-N18	-147.1

Bond lengths, bond angles and dihedral angles of the $Cu(BOX)_2H_2O$ and $Mn(BOX)_2H_2O$ complexes were quite similar. Slight elongations were observed in the aromatic and aliphatic carbon-carbon bond lengths, with the formation of the complexes. But the C14-N18 (1.368 Å) bond between the oxime and amine groups elongated significantly with the complex formation. For both complexes, C14-N18 bond length was 1.485 Å and 1.497 Å, respectively. Due to the electron donation of N18 to the metal ion, the charge density decreased and the bond with the oxime carbon was weakened and elongated. In addition, the N15-O17 bond length of 1.419 Å in the HBOX ligand was shortened in the complexes and was calculated as 1.358 Å (N43-O52) and 1.361 Å (N43-O52) for $Cu(BOX)_2H_2O$ and $Mn(BOX)_2H_2O$ complexes, respectively. The reason of this shortening in the nitrogen-oxygen bond was interpreted as backbonding. With the backbonding interaction, the metal ions in the complexes donated the electron density back to the ligand and the nitrogen-oxygen bond in oxime group was shortened by strengthening.

From the angles around the Cu(II) and Mn(II), two oxime oxygen and amine nitrogen atoms were not lying in same plane. The coordination water was bound perpendicular to the metal ion. The resulting bond distances and angles for the $Cu(BOX)_2H_2O$ and $Mn(BOX)_2H_2O$ complexes were consistent with a pentacoordinate distorted square-pyramidal structure involving the amine nitrogen atom, deprotonated oxime oxygen atom and coordination water.

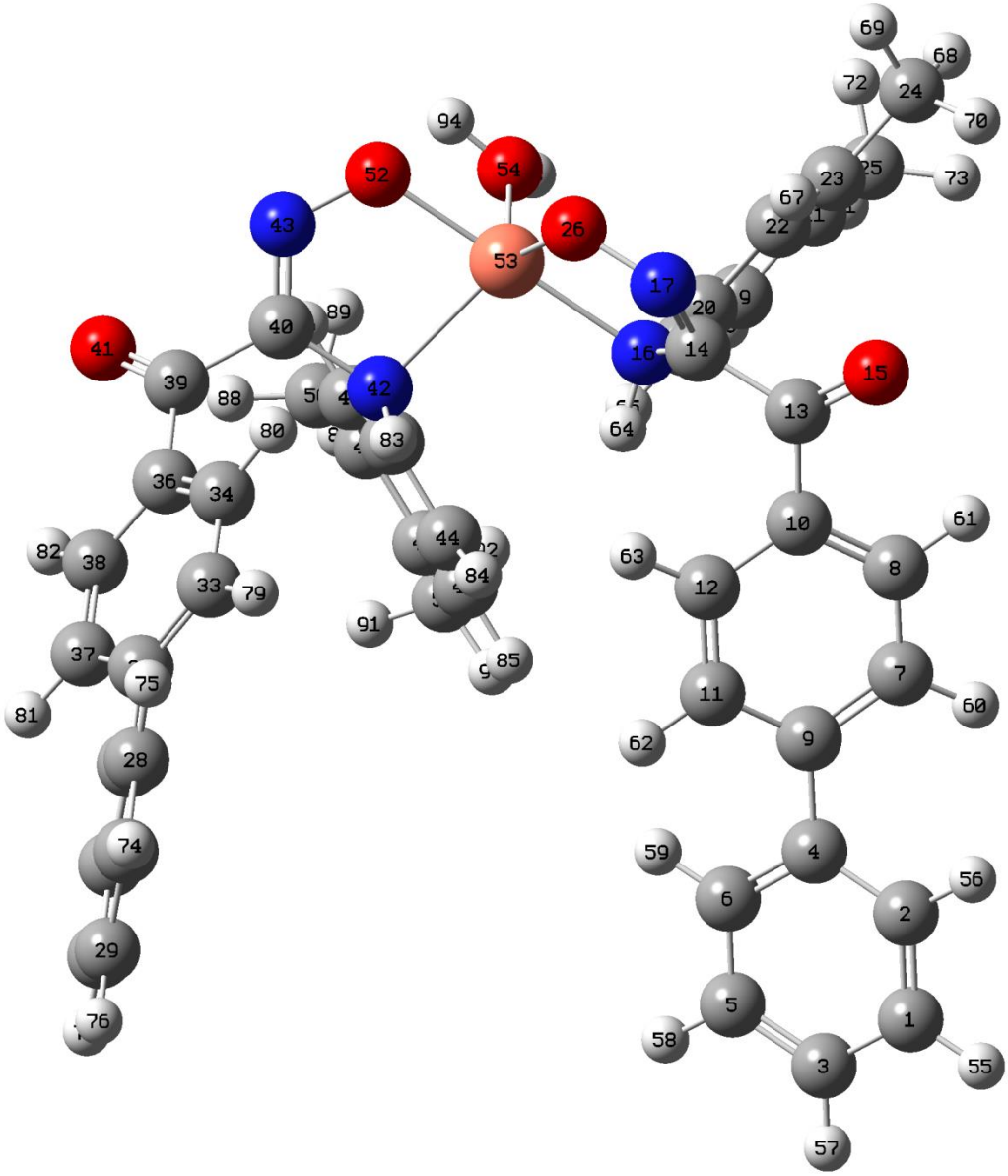

Figure 10. The optimized geometric structure of the $Cu(BOX)_2H_2O$ computed at B3LYP/LANL2DZ level

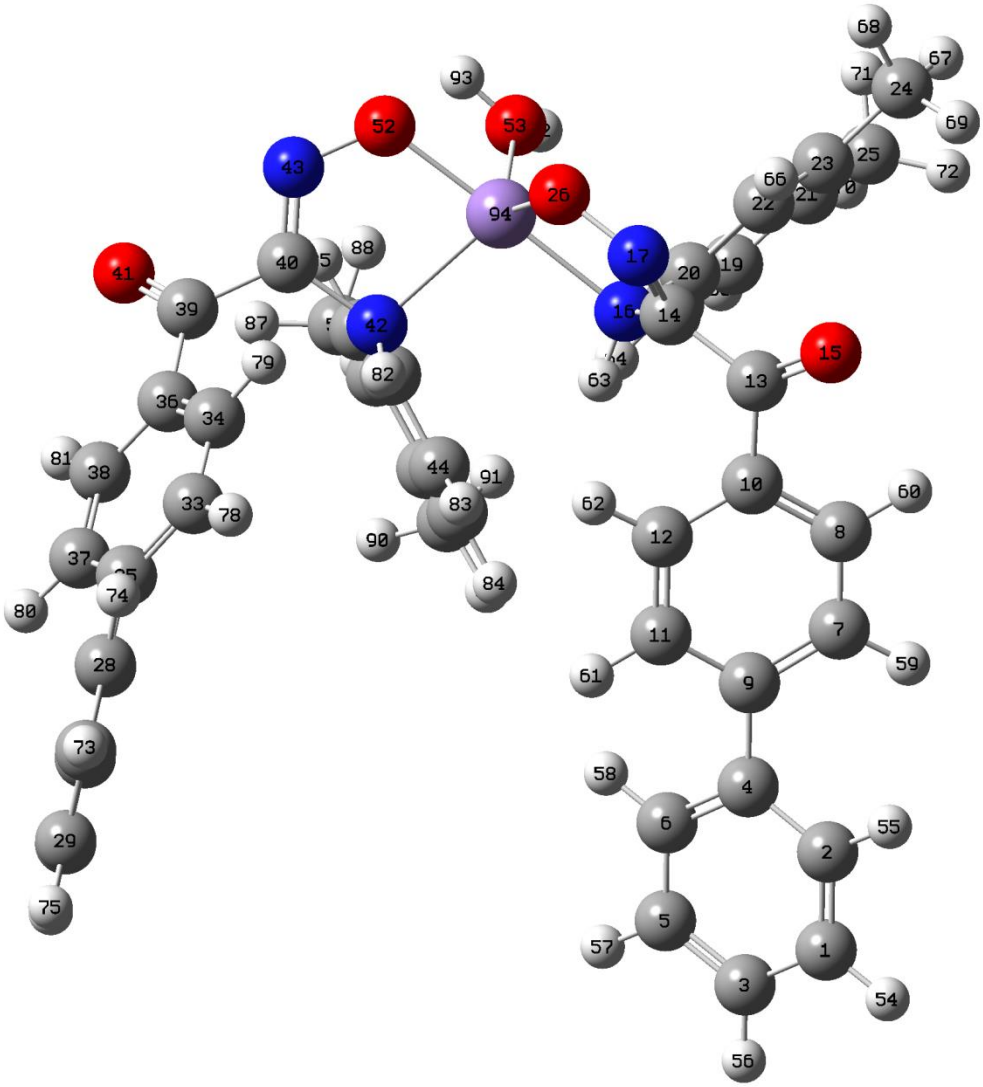

Figure 11. The optimized geometric structure of the $Mn(BOX)_2H_2O$ computed at B3LYP/LANL2DZ level

Table 9. Some selected calculated bond lengths (Å), bond and dihedral angles (^{o}) for the $Cu(BOX)_2H_2O$ and $Mn(BOX)_2H_2O$ computed at B3LYP/LANL2DZ level

$Cu(BOX)_2H_2O$		**$Mn(BOX)_2H_2O$**	
Parameters	**B3LYP/ LANL2DZ**	**Parameters**	**B3LYP/ LANL2DZ**
Bond lengths (Å)			
C27-C28	1.405	C27-C28	1.405
C37-C38	1.402	C37-C38	1.401
C1-C2	1.406	C1-C2	1.406
C11-C12	1.403	C11-C12	1.403
C30-C35	1.490	C30-C35	1.490
C4-C9	1.491	C4-C9	1.491
C29-H76	1.087	C29-H75	1.087
C3-H57	1.087	C3-H56	1.087
C36-C39	1.494	C36-C39	1.497
C10-C13	1.500	C10-C13	1.500
C39-O41	1.253	C39-O41	1.254
C13-C14	1.495	C13-C14	1.496
C40-N43	1.306	C40-N43	1.310
C14-N16	1.485	C40-N43	1.497
N43-O52	1.358	N43-O52	1.361
O52-Cu53	1.975	O52-Mn94	1.975
N42-Cu53	2.228	N42-Mn94	2.283
Cu53-O54	2.132	Mn94-O53	2.122
O26-Cu53	1.990	O26-Mn94	2.028
N16-Cu53	2.100	N16-Mn94	2.134
N42-C46	1.450	N42-C46	1.450
C18-C19	1.405	C18-C19	1.406
Bond angles (^{o})			
C27-C29-C31	119.4	C27-C29-C31	119.4
C32-C30-C35	121.0	C32-C30-C35	120.9
C34-C36-C38	118.9	C34-C36-C38	118.8
C36-C39-O41	121.9	C36-C39-O41	121.5

C40-N43-O52	118.8	C40-N43-O52	118.3
N42-Cu53-O52	79.9	N42-Mn94-O52	79.9
N16-Cu53-O26	82.4	N16- Mn94-O26	81.1
O54-Cu53-N16	100.6	O53- Mn94-N16	102.1
C18-C20-C22	120.1	C18-C20-C22	120.2
Dihedral angles (^{o})			
C29-C31-C32-C30	0.1	C29-C31-C32-C30	0.1
C32-C30-C35-C33	-146.5	C32-C30-C35-C33	-146.6
C38-C36-C39-C40	-152.7	C38-C36-C39-C40	-152.6
O41-C39-C40-N43	49.2	O41-C39-C40-N43	49.1
C36-C39-C40-N42	50.3	C36-C39-C40-N42	50.3
C40-N42-C46-C44	-149.0	C40-N42-C46-C44	-149.2
N17-O26-Cu53-N42	90.9	N17-O26-Mn94-N42	89.0

The calculation of the Mulliken atomic charges of a molecule provides important information in explaining the structure. The distribution of calculated Mulliken atomic charge values of the HBOX is presented in Fig. 12. Mulliken atomic charges of O16 and O17 atoms in the carbonyl and oxime groups were calculated as -0.456362 and -0.443475 a.u., respectively. These negative charges were due to the high electronegativity of the oxygen atom. The highest negative charge in the HBOX was computed on N18 atom with -0.650188 a.u. The reason for the highest negative charge of this nitrogen atom adjacent to the benzene ring might be originated from the hyperconjugation effect of two methyl groups bound to *m*- and *p*- positions of benzo ring. The calculation of the C25 and C26 atomic charges as negative values also supported the hyperconjugation effect. The methyl groups containing these carbon atoms donated charge to the benzene ring, which allowed the nitrogen atom adjacent to the benzene to become rich as a negative charge. On the contrary, the highest positively

charged carbon atoms were C14 (0.443080 a.u.) and C13 (0.360059 a.u.) due to their bonding to oxime and carbonyl atoms, respectively.

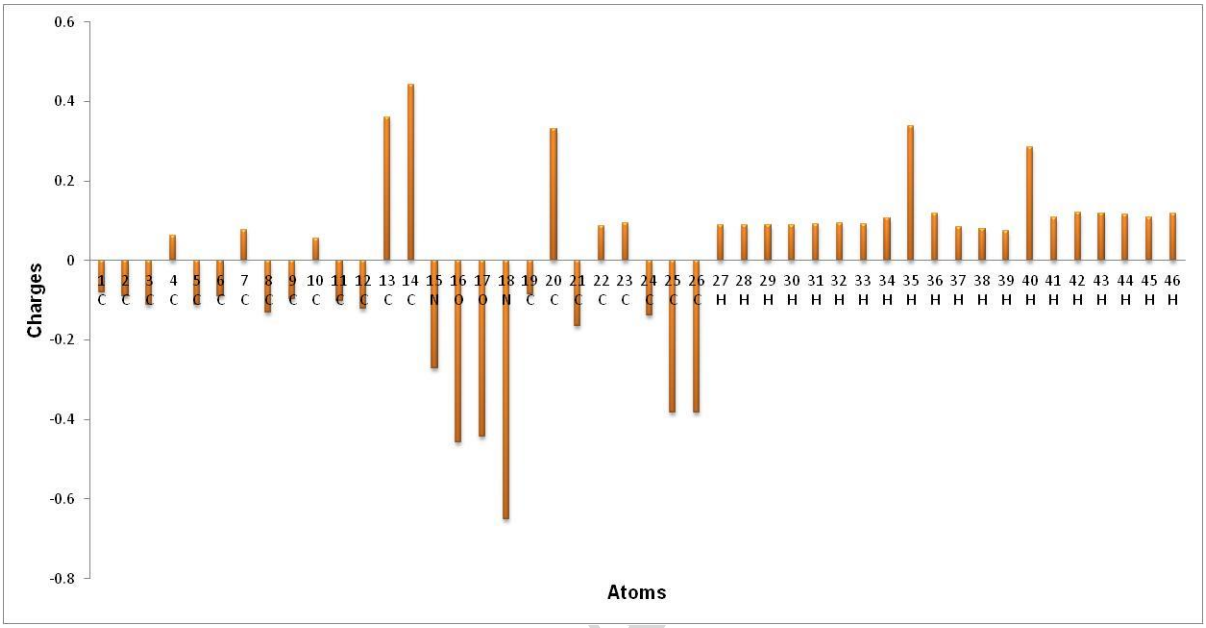

Figure 12. Mulliken atomic charges of the HBOX computed at B3LYP/6-311G(d,p) level

3.7.2. Molecular Electrostatic Potential (MEP) Diagram

Electrostatic potential energy maps represent the charge distributions of molecules in three dimensions. These maps enable us to visualize the variable charged regions of a molecule. Information about charge distributions in the molecule can be used to determine how molecules interact with each other. The different colours in these diagrams are indicative of the different electronic potential regions in the molecule. The red regions of a MEP diagram show the electron-rich regions of a molecule, while the blue parts define the most electron-poor regions of a molecule. In addition green colour areas represent the regions of zero potential. The red and blue regions of MEP surface diagrams are related to the electrophilic and nucleophilic reactivity of the molecule, respectively. As can be seen from Fig. 13, electron-rich region in the structure of the HBOX was mainly located on the oxygen atom

(O16) of the carbonyl group. A slight negative charge density on the N18 atom of the amine group of HBOX was also observed. The positive area of MEP surface of title molecule was localized on the hydrogen atoms of the oxime and amine groups. Electron density values of H40 in oxime group and H35 in amine group was calculated as 0.338184 and 0.285586 a.u., respectively. This result also explained the occurrence of deprotonation of the oxime group in complexation instead of the proton of amine group. In the synthesis of the complex, the pH of the medium was kept between 5.5-6 and more acidic H35 was removed from the oxime group. Thus, the formed anionic oxygen atom produced a stronger attack towards the metal ions than the neutral oxygen atom of the oxime group.

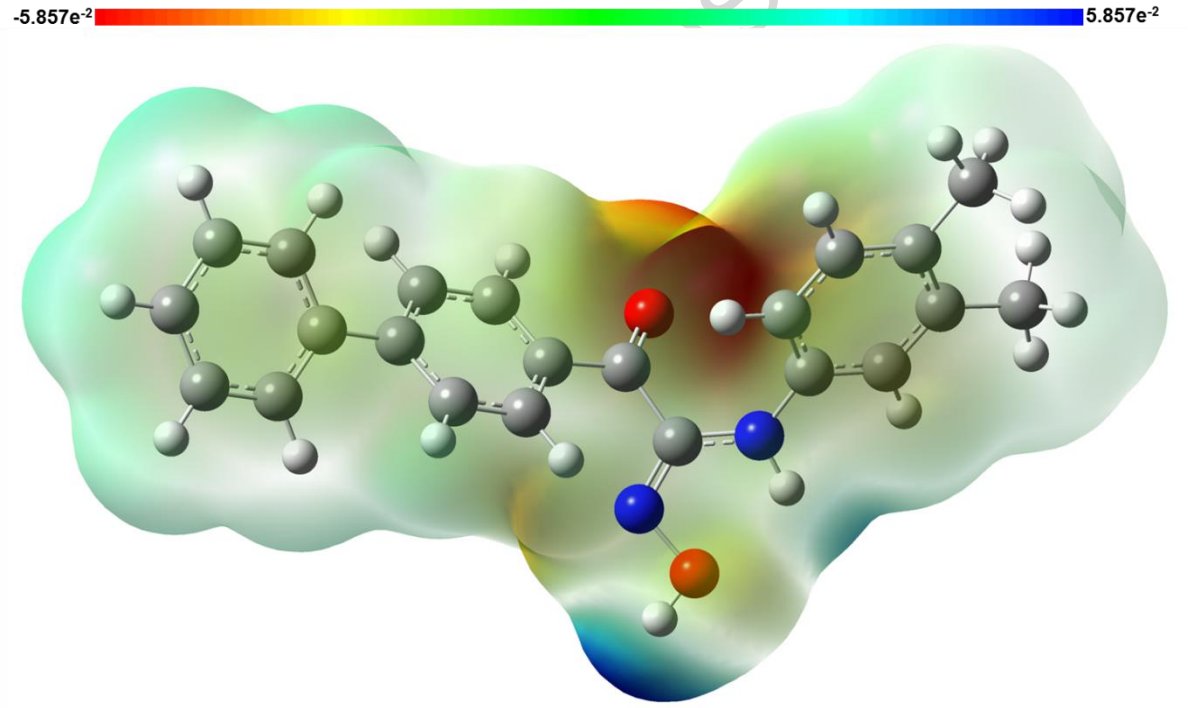

Figure 13. MEP surface diagram of the HBOX computed at B3LYP/6-311G(d,p) level

3.7.3. Conformational Analyses

Theoretical calculations was performed using B3LYP/6-311G (d,p) level to find the most stable and unstable conformations of the HBOX molecule. Potential energy surface diagram was computed on the rotations of τ_1 = C10-C13-C14-N18 and τ_2 = C13-C14-N18-C20

dihedral angles, scanning from -180◦ to 180◦ in steps of 10^{o} (Fig. 14). From calculations, it was found that the structure of the HBOX molecule had three local minima with -1110.0130 a.u. (-696543.82 kcal/mol, C1), -1110.0133 a.u. (-696544.01 kcal/mol, C2) and -1110.0136 a.u. (-696544.20 kcal/mol, C3), respectively.

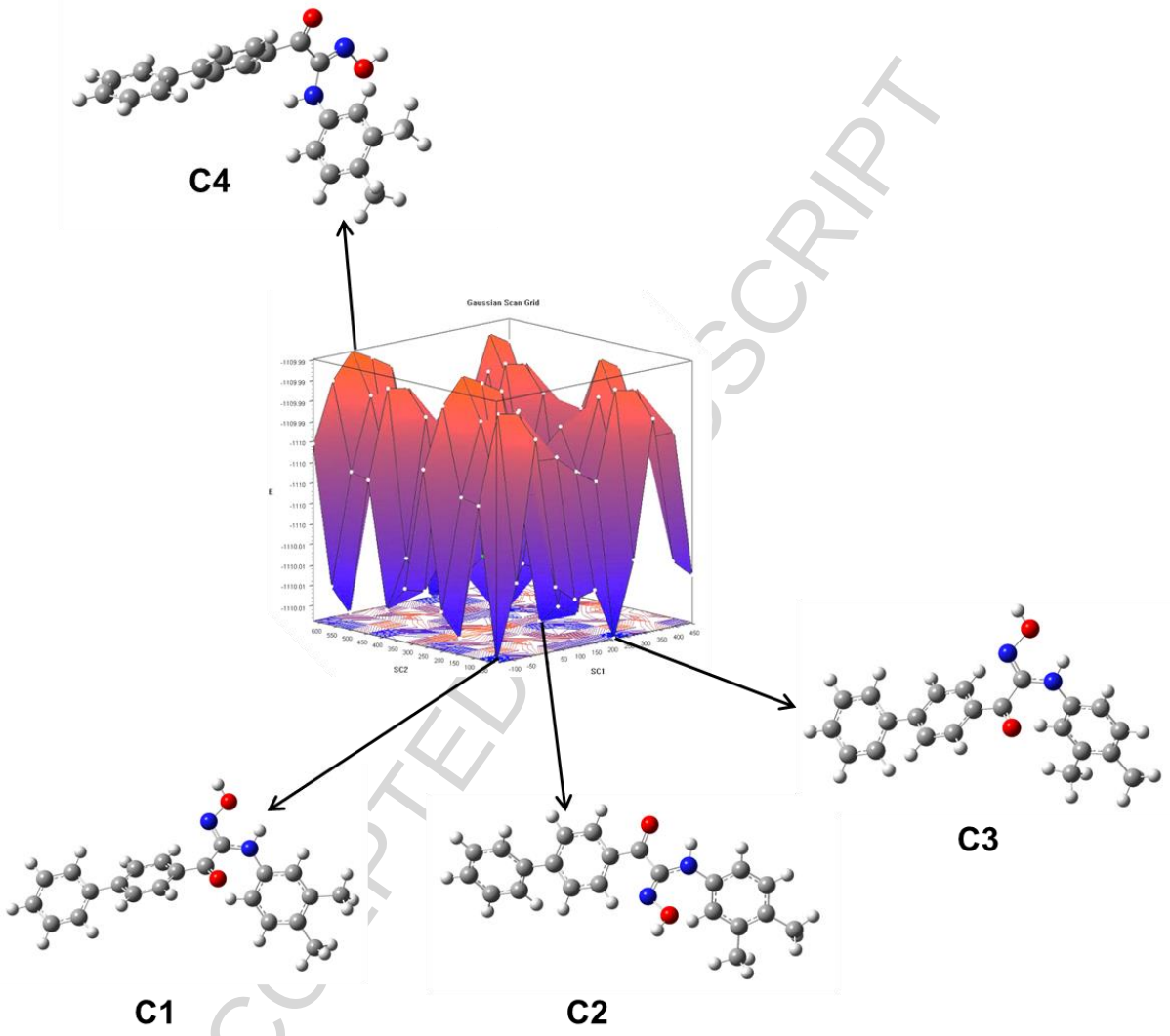

Figure 14. Potential energy surface diagram of the HBOX computed at B3LYP/6-311G(d,p) level. Relevant conformations were labelled as C1, C2, C3 and C4.

The energy of the most unstable conformer (C4) of the HBOX molecule was found to be -1109.9903 a.u. (-696529.58 kcal/mol, C4). Overall of all, conformer C3 had the least relative energy and most stable. The difference between the most stable (C3) and unstable (C4)

conformers of HBOX calculated using two dihedral angles was 14.62 kcal/mol. The structure of the unstable C4 conformer showed that the carbonyl and oxime group were predominantly in *cis*- position. For this reason, the biphenyl and methylated aromatic amine groups, which were the two bulky moieties in the HBOX molecule, were closer to each other and the title molecule became more unstable due to the steric effect. However, since in the C3 conformer neither the carbonyl-oxime pair nor the biphenyl- methylated aromatic amine pair existed in the same plane, the steric hindrance was reduced and the HBOX molecule became more stable.

3.8. Molecular Docking Studies

Dimethylaniline bearing ketooxime ligand (HBOX) was tested for its antiangiogenic and antilymphangiogenic properties by molecular docking study. HBOX bound to 1CX2 protein with 2 hydrogen bonds at the lowest energy level which indicates the most stabilized form of the protein ligand complex. The ligand also bound to 2XIR with two hydrogen bonds at the lowest energy level, the highest full fitness score and released energy (Fig. 16). These energy levels were chosen by checking each cluster's minimum molecular energy, full fitness score and free Gibbs energy (Table 10). Fig. 15 shows the HBOX-1CX2 complex bounded with minimum energy in ribbon and space filled structure.

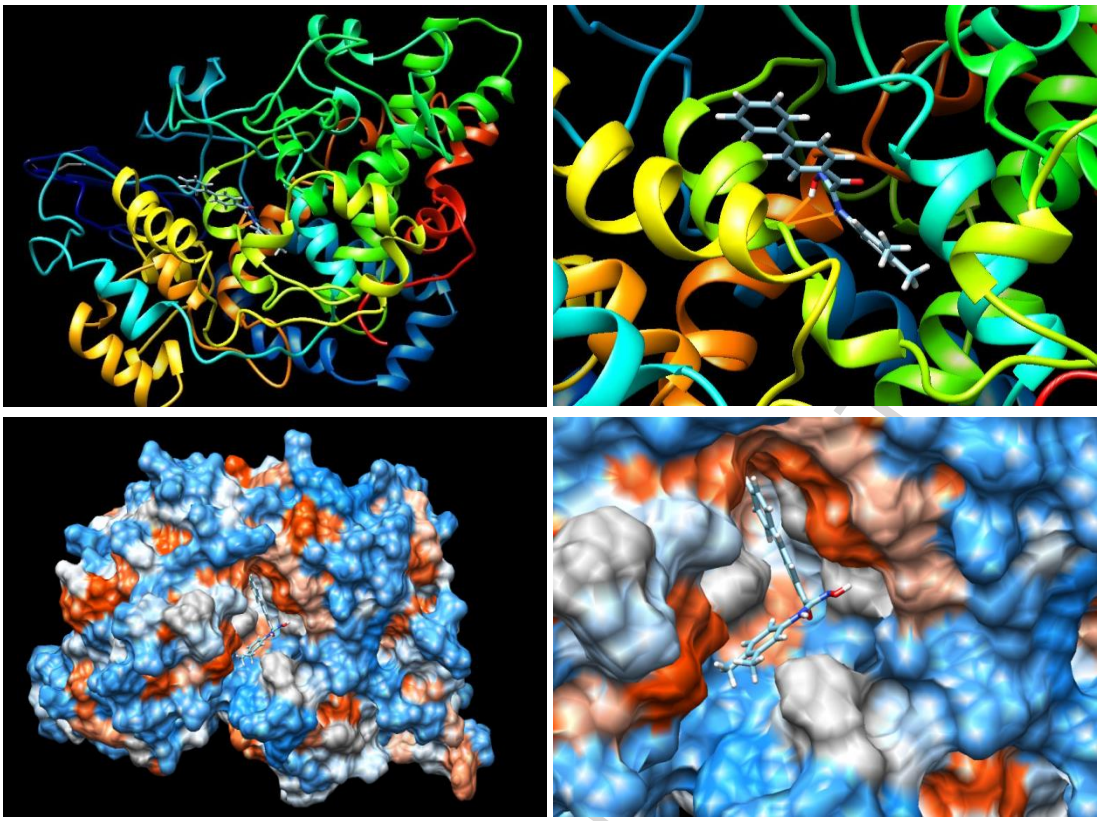

Figure 15. 1CX2 and HBOX complex shown in ribbon (above) and space filled structure (below).

The binding energies with minus values confirm the spontaneous docking. The HBOX-1CX2 complex has a -8.54 while the HBOX-2XIR has -8.35 kcal/mol of ΔG value. HBOX-1CX2 has two hydrogen bonds between NH and OH of the HBOX ligand and O of Tyr 385 of the 1CX2 enzyme. Similarly, HBOX-2XIR has also two hydrogen bonds between C=O of the HBOX and NH of Cys 1024 and OH of the HBOX and NH of Lys 1025 of the 2XIR protein (Fig. 16).

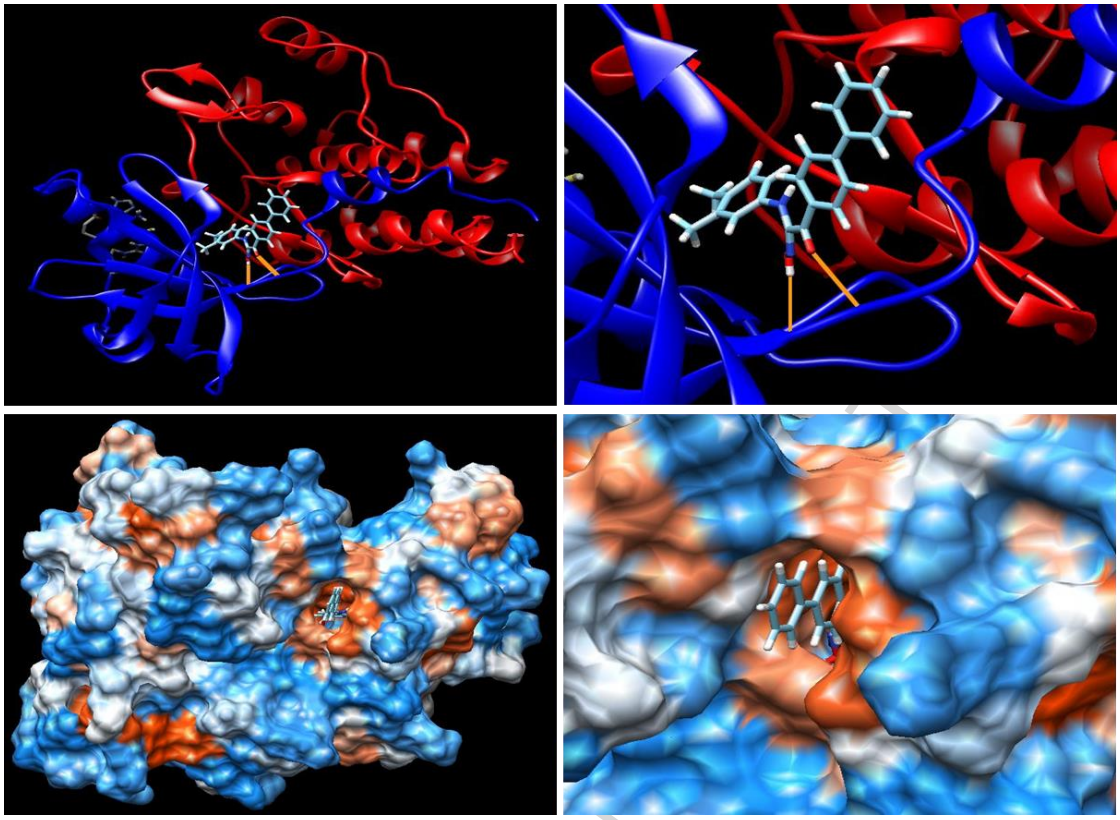

Figure 16. 2XIR and HBOX complex shown in ribbon (above) and space filled structure (below).

Table 10. Full fitness score, binding energy and hydrogen bond information between the ligand-target molecule couples

Ligand-Target	Full fitness score (kcal/mol)	ΔG (kcal/mol)	H Bond Location (Length)
HBOX-1CX2	-2369.06 (Energy: 41.65)	-8.54	NH of ligand & O of Tyr 385 (2.225 Å) OH of ligand & O of Tyr 385 (2.573 Å)
HBOX-2XIR	-1547.03 (Energy: 44.35)	-8.35	C=O of ligand & NH of Cys 1024 (2.489 Å) OH of oxime & NH of Lys 1025 (2.243 Å)

3.9. Enzymatic Activity Studies

3.9.1. Catecholase-Like Enzyme Activity

The catalytic oxidation of 3,5-di-*tert*-butylcatechol (3,5-DTBC) to the 3,5-di-*tert*-butyl-*o*-benzoquinone (3,5-DTBQ) was studied to investigate the catecholase-like activity of the $Cu(BOX)_2H_2O$ and $Mn(BOX)_2H_2O$ complexes (Fig. 17). The time dependent formations of 3,5-DTBQ (λ_{max} = 400 nm) in the presence of Cu(II) and Mn(II) complexes are illustrated in Fig. 18 and 19. Both complexes showed a moderate catecholase-like activity in oxygen-saturated methanolic solution. Copper and manganese metals were used for complex design for their relatively easier reducibility.

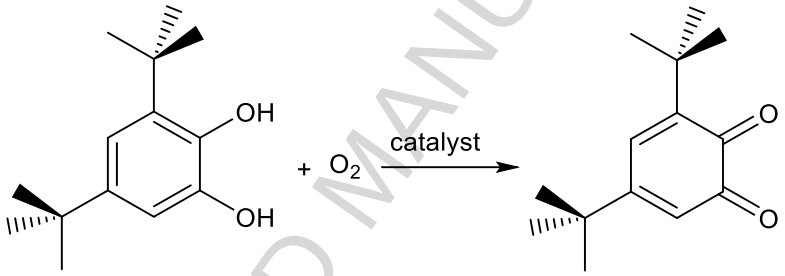

Figure 17. Formation of 3,5-di-*tert*-butyl-o-benzoquinone from 3,5-di-*tert*-butylcatechol

Distortion in the geometry of the complexes increases the catalytic activity [62-64]. The distorted square-pyramidal structures might contribute the catalytic efficiency of the complexes. The observed rate constant values (k_{obs}) of the metal complexes for the formation of 3,5-DTBQ were calculated from the $\ln(A_\infty/A_\infty-A_t)=kt$ equation. A_∞ and A_t were the absorbance of the formed 3,5-DTBQ at time $t = \infty$ and $t = t$, respectively [65]. As can be seen from Fig. 18, the observed rate constant for the $Cu(BOX)_2H_2O$ and $Mn(BOX)_2H_2O$ were found to be 0.0730 and 0.1146 s^{-1}, respectively (Table 11). Mn(II) complex showed a higher catecholase-like activity compared to the Cu(II) complex of the HBOX. Higher catalytic activity of the $Mn(BOX)_2H_2O$ might be related to the better reducible potential of Mn(II)

compared to Cu(II) and a better proximity with 3,5-DTBC, which was reported previously [66].

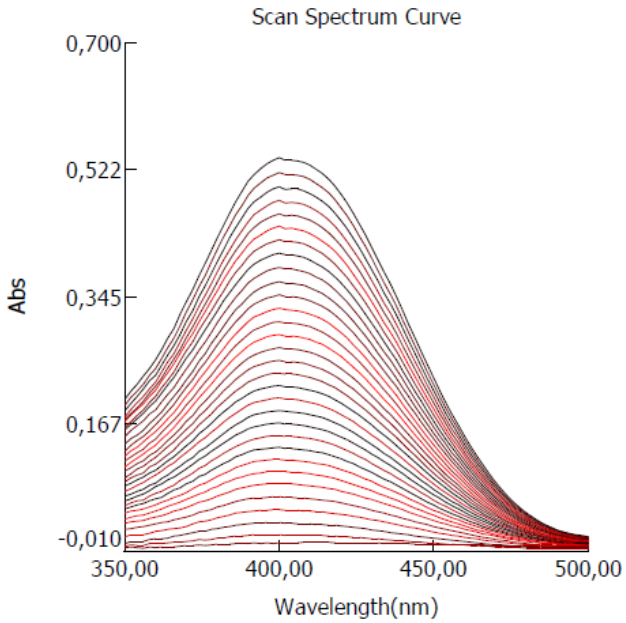

Figure 18. The increase of absorbance followed at 400 nm due to the formation of 3,5-DTBQ by $Cu(BOX)_2H_2O$ catalysis

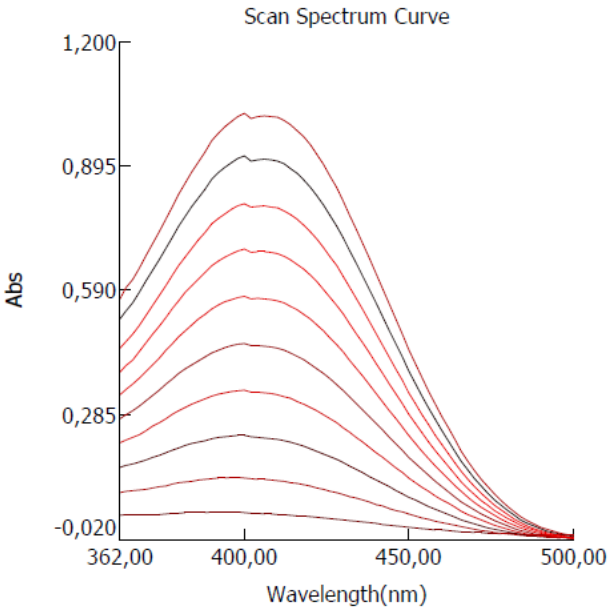

Figure 19. The increase of absorbance followed at 400 nm due to the formation of 3,5-DTBQ by $Mn(BOX)_2H_2O$ catalysis

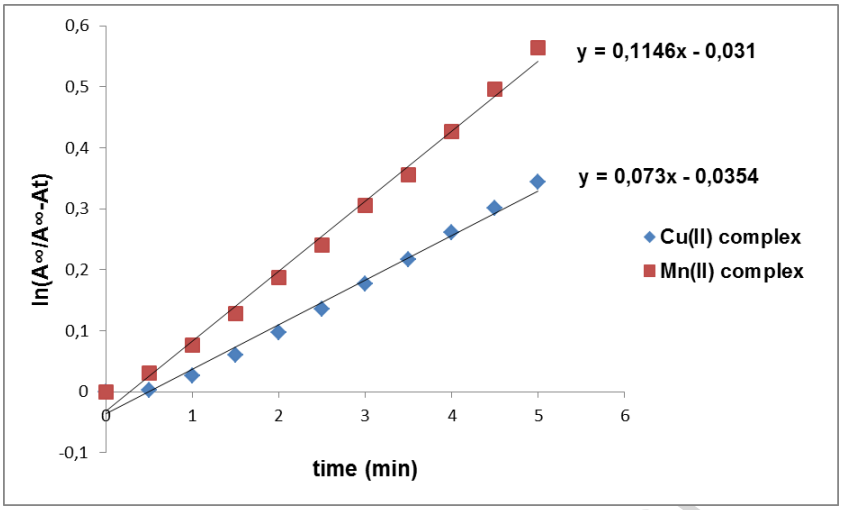

Figure 20. Comparison of Cu(II) and Mn(II) complexes' k_{obs} values

3.9.2. Phenoxazinone Synthase-Like Enzyme Activity

The phenoxazinone synthase-like enzymatic activities of the $Cu(BOX)_2H_2O$ and $Mn(BOX)_2H_2O$ were studied with the help of electronic spectroscopy by monitoring the appearance of the absorbance maximum of the 2-aminophenoxazine-3-one (APX) (Fig. 21). This oxidation reaction of the OAPH wasn't occurred in the absence of the complex. It was found that both of the complexes showed phenoxazinone synthase-like activity. The time dependent formations of APX (λ_{max} = 433 nm) in the presence of the Cu(II) and Mn(II) are presented in Fig. 22 and 23.

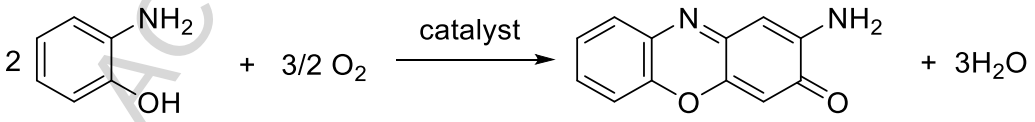

Figure 21. Formation of 2-aminophenoxazine-3-one from 2-aminophenol

In order to find out the observed reaction rate (k_{obs}) between OAPH and synthesized metal complexes, time dependent change was studied at 433 nm. The k_{obs} was determined from the slope of the plot in Fig. 24. The rate constant values for the $Cu(BOX)_2H_2O$ and

$Mn(BOX)_2H_2O$ were found to be 0.0671 and 0.2673 s^{-1}, respectively (Table 11). According to these k_{obs} values, $Mn(BOX)_2H_2O$ was better catalyst than the $Cu(BOX)_2H_2O$ complex. Both of the complexes were synthesized from the same ligand and these complexes had similar geometry. The higher catalytic activity of the Mn(II) complex than can be explained by the relatively higher oxidation and reduction potential of the Mn(II) ion in the heart of the complex structure.

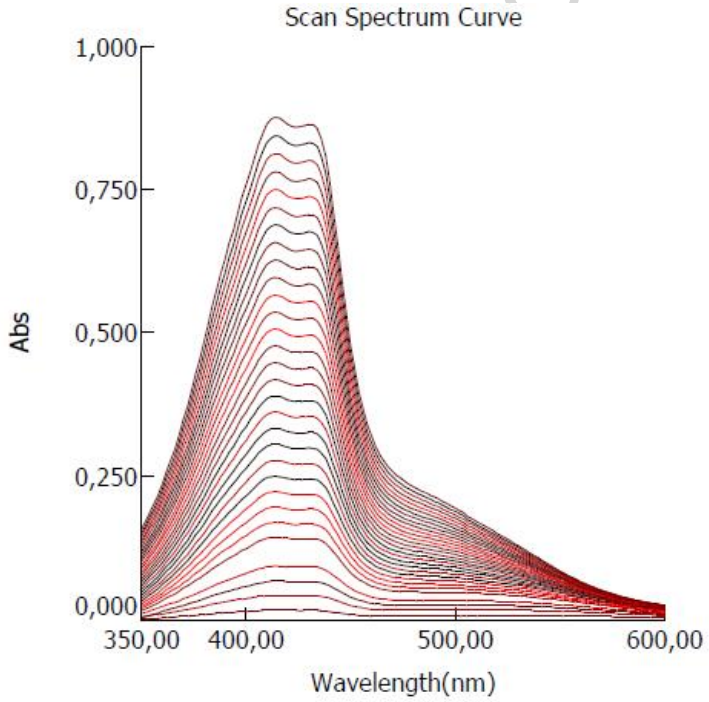

Figure 22. The increase of absorbance followed at 433 nm due to the formation of APX by $Cu(BOX)_2H_2O$ catalysis

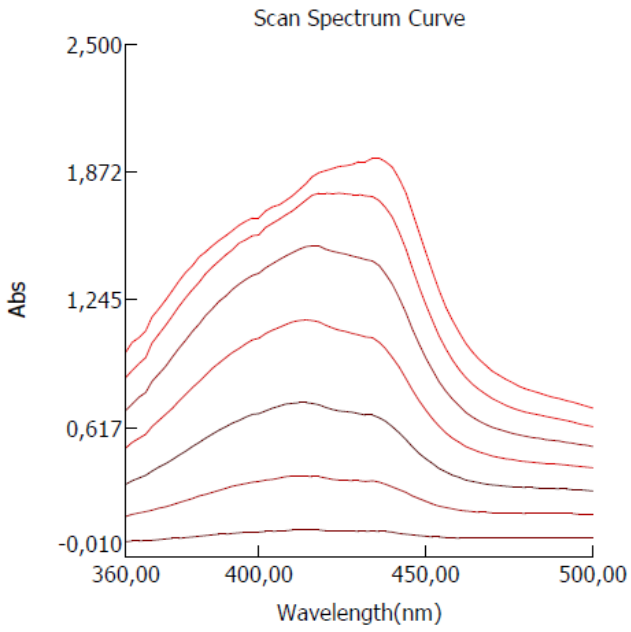

Figure 23. The increase of absorbance followed at 433 nm due to the formation of APX by $Mn(BOX)_2H_2O$ catalysis

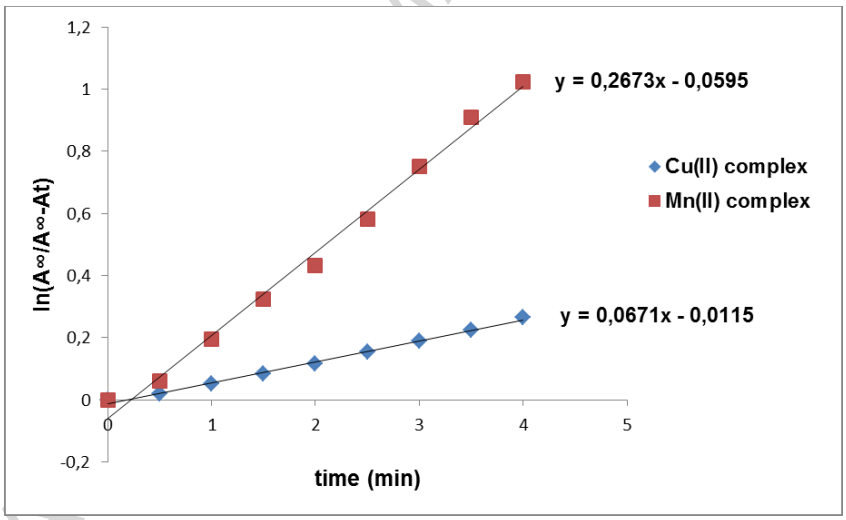

Figure 24. Comparison of Cu(II) and Mn(II) complexes' k_{obs} values

Table 11. Observed reaction rate (k_{obs}, s^{-1}) values of the complexes

Complex	Catecholase-like activity	Phenoxazinone synthase-like activity
$Cu(BOX)_2H_2O$	0.0730	0.0671
$Mn(BOX)_2H_2O$	0.1146	0.2673

Conclusion

A novel molecule 2-([1,1'-biphenyl]-4-yl)-N-(3,4-dimethylphenyl)-N'-hydroxy-2-oxoacetimidamide (HBOX) and its mononuclear Cu(II) and Mn(II) complexes were synthesized. Elemental analyses, stoichiometric and spectroscopic studies discussed above indicated that, the HBOX was acted as a bidentate ligand and coordinated to the metal ions through the nitrogen atom of the amine and deprotonated oxygen atom of oxime groups. The metal:ligand ratio was found to be 1:2. The geometric parameters, ^{1}H- and ^{13}C-NMR chemical shifts, vibrational wavenumbers, Uv-vis wavelengths were calculated using DFT method with B3LYP/6-311G(d,p) and B3LYP/LANL2DZ for the HBOX and its metal complexes, respectively. MEP, Mulliken atomic charge, PES and conformer analyses were also performed. The calculated data were in good agreement with the experimental results. HBOX was also investigated for its inhibitory effect against angiogenic factors VEGFR-2 and COX-2 by molecular docking study. Docking studies were revealed that the HBOX ligand had a potential for binding VEGFR-2 and COX-2, and eventually use in antiangiogenesis and antilymphoangiogenesis therapy. Furthermore, two enzymatic activities of the $Cu(BOX)_2H_2O$ and $Mn(BOX)_2H_2O$ complexes were investigated. It was found that both complexes showed significant catalytic activity for oxidation of 3,5-di-*tert*-butylcatechol (catecholase-like activity) and 2-aminophenol (phenoxazinone synthase-like activity). However, $Mn(BOX)_2H_2O$ showed better activity with k_{obs} = 0,1146 and 0,26733 s^{-1} values in both enzymatic activity studies. The ΔE value between the HOMO and LUMO of the

$Mn(BOX)_2H_2O$ was lower than the $Cu(BOX)_2H_2O$ complex which indicated a relatively easier electron transfer between the orbitals resulting in a higher reactivity and catalytic activity. Namely, $Mn(BOX)_2H_2O$ is softer than $Cu(BOX)_2H_2O$.

REFERENCES

[1] Smith AG, Tasker PA, White DJ (2003) The structures of phenolic oximes and their complexes. Coordin Chem Rev 241(1-2):61-85.

[2] Chakravorty A, (1974) Structural chemistry of transition metal complexes of oximes. Coordin Chem Rev 13:1-46.

[3] Cox, P. A. (2010). Transition metal oxides: an introduction to their electronic structure and properties (Vol. 27). Oxford University Press.

[4] Dong Z, Luo Q, Liu J (2012) Artificial enzymes based on supramolecular scaffolds. Chem Soc Rev 41(23):7890-7908.

[5] Paschke J, Kirsch M, Korth HG, de Groot H, Sustmann R (2001) Catalase-like activity of a non-heme dibenzotetraaza [14] annulene-Fe(III) complex under physiological conditions. J Am Chem Soc 123(44):11099-11100.

[6] Xu Z, Zhou L (2011) A DFT study of a novel oxime anticancer trans platinum complex: Monofunctional and bifunctional binding to purine bases. Int J Quantum Chem 111(9):1907-1920.

[7] Banday AH, Akram SMM, Shameem SA (2014) Benzylidine pregnenolones and their oximes as potential anticancer agents: Synthesis and biological evaluation. Steroids 84:64-69.

[8] Ichimaru Y, Fujii T, Saito H, Sano M, Uchiyama T, Miyairi S (2017) 5-Bromoindirubin 3′-(O-oxiran-2-ylmethyl) oxime: A long-acting anticancer agent and a suicide inhibitor for epoxide hydrolase. Bioorgan Med Chem 25(17):4665-4676.

[9] Qin Y, Qiang S, Ji S, Liu Z, Hu C, Ma S (2018) Synthesis and antibacterial activity of novel 3-O-arylalkylcarbamoyl-3-O-descladinosyl-9-O-(2-chlorobenzyl) oxime clarithromycin derivatives. Bioorgan Med Chem Lett 28(20):3324-3328.

[10] Bharathi S, Wong PT, Desai A, Lykhytska O, Choe, V., Kim, H., Thomas TP, Baker Jr JR, Choi SK (2014) Design and mechanistic investigation of oxime-conjugated PAMAM dendrimers as the catalytic scavenger of reactive organophosphate. J Mater Chem B 2(8):1068-1078.

[11] Wang R, Zhang X, Song H, Zhou S, Li S (2014) Synthesis and evaluation of novel alkannin and shikonin oxime derivatives as potent antitumor agents. Bioorg Med Chem Lett 24(17):4304-4307.

[12] Carmeliet P, Jain RK (2000) Angiogenesis in cancer and other diseases. Nature, 407(6801):249-257.

[13] Tammela T, Zarkada G, Wallgard E, Murtomäki A, Suchting S, Wirzenius M, Waltari M, Hellström M, Schomber T, Peltonen R, Freitas C, Duarte A, Isoniemi H, Laakkonen P, Christofori G, Ylä-Herttuala S, Shibuya M, Pytowski B, Eichmann A, Betsholtz C, Alitalo K (2008) Blocking VEGFR-3 suppresses angiogenic sprouting and vascular network formation. Nature, 454(7204):656-660.

[14] Ferrara N, Gerber HP, LeCouter J (2003) The biology of VEGF and its receptors. Nat Med 9(6):669-676.

[15] Ellis LM, Hicklin DJ (2008) VEGF-targeted therapy: Mechanisms of anti-tumour activity. Nat Rev Cancer 8(8):579-591.

[16] Huh JE, Kang JW, Nam D, Baek YH, Choi DY, Park D S, Lee JD (2012) Melittin suppresses VEGF-A-induced tumor growth by blocking VEGFR-2 and the COX-2-mediated MAPK signaling pathway. J Nat Prod 75(11):1922-1929.

[17] Kitchen DB, Decornez H, Furr JR, Bajorath J (2004) Docking and scoring in virtual screening for drug discovery: Methods and applications. Nat Rev Drug Discov 3(11):935-49.

[18] Doss CGP, Chakraborty C, Narayan V, Kumar DT (2014) Computational approaches and resources in single amino acid substitutions analysis toward clinical research. In Adv Protein Chem Str Bio 94:365-423. Academic Press.

[19] Yu F, Cangelosi VM, Zastrow ML, Tegoni M, Plegaria JS, Tebo AG, Mocny CS, Ruckthong L, Qayyum H, Pecoraro VL (2014) Protein design: Toward functional metalloenzymes. Chem Rev 114(7):3495-3578.

[20] Peck EM, Smith BD, (2015) Synthetic receptors for biomolecules: Design principles and applications. RSC Publications, UK.

[21] Metal Complexes May be Better Anticancer Drugs. (1982) Chem Eng News, 19 April, p. 36

[22] Asif M (2017) Review on to free radicals, antioxidants and brief overview of oximes, Int J Curr Res Appl Chem & Chem Eng 3(1):44-67.

[23] Görgülü G, Dede B (2018) Catalase, catecholase and phenoxazinone synthase-like activities of homodinuclear Co(II), Ni(II), Cu(II) and Zn(II) complexes including oxime group. J Chil Chem Soc 63(3):4072-4076.

[24] Serbest K, Göktekin Ö, Karaoğlu K, Zengin A, Çoruh U (2018) Oxime derivative unsymmetrical azine, its Ni(II), Cu(II) and Zn(II) complexes: Synthesis, spectroscopy and catecholase activity. Heteroatom Chem e21439.

[25] Erdem-Tunçmen M, Karipcin F, Atiş M, Perçin-Özkorucuklu S (2014) New organocobaloxime derivatives-Synthesis, characterization, catalase-like activity and DFT studies. J Organomet Chem 756:10-18.

[26] Görgülü G, Dede B (2018) Enzymatic activities of a novel dinuclear Cu(II)-Ni(II) complex: Design, synthesis and characterization. Fresen Environ Bull 27(6):3958-3964.

[27] Barthelmes J, Ebeling C, Chang A, Schomburg I, Schomburg D (2007) BRENDA, AMENDA and FRENDA: The enzyme information system in 2007. Nucleic Acids Res 35(suppl_1):D511-D514.

[28] Long LM, Henze HR (1941) Synthesis of ketone derivatives of biphenyl by the Friedel-Crafts reaction[1], J Am Chem Soc 63:1939-1940.

[29] Karipcin F, Arabalı F (2006) Synthesis and characterization of new ketooximes and their complexes. Russ J Inorg Chem 51(9):1467-1472.

[30] Karataş I, Uçan HI (1998) The synthesis of biphenylglyoxime and bis(phenylglyoxime) and their complexes with Cu(II), Ni(II) and Co(II). Synth React Inorg Met Org Chem 28:383-391.

[31] Gaussian 09, Revision E.01, Frisch MJ, Trucks GW, Schlegel, HB et al (2016) Gaussian, Inc., Wallingford CT.

[32] Becke AD (1993) Becke's three parameter hybrid method using the LYP correlation functional. J Chem Phys 98:5648-5652.

[33] Lee C, Yang W, Parr RG (1988) Development of the Colle-Salvetti correlation-energy formula into a functional of the electron density, Phys. Rev. B 37:785-789.

[34] GaussView, Revision 5.0.9 (2009) Dennington R, Keith TA, Millam JM, Semichem Inc., Shawnee Mission, KS.

[35] O'Boyle NM, Tenderholt AL, Langner KM (2008) cclib: A library for package-independent computational chemistry algorithms. J Comp Chem 29(5): 839-845.

[36] Ditchfield R (1972) Molecular orbital theory of magnetic shielding and magnetic susceptibility. J Chem Phys 56(11):5688-5691.

[37] Wolinski K, Hinton JF, Pulay P (1990) Efficient implementation of the gauge-independent atomic orbital method for NMR chemical shift calculations. J Am Chem Soc 112(23):8251-8260.

[38] Grosdidier A, Zoete V, Michielin O, (2011) SwissDock, a protein-small molecule docking web service based on EADock DSS. Nucleic Acids Res 39:270-277.

[39] Pettersen EF, Goddard TD, Huang CC, Couch GS, Greenblatt DM, Meng EC, Ferrin TE (2004) UCSF Chimera-a visualization system for exploratory research and analysis. J Comput Chem 13:1605-1612.

[40] Reim J, Krebs B (1997) Synthesis, structure and catecholase activity study of dinuclear copper (II) complexes. J Chem Soc Dalton 20:3793-3804.

[41] Kaizer J, Baráth G, Csonka R, Speier G, Korecz L, Rockenbauer A, Párkányi L (2008) Catechol oxidase and phenoxazinone synthase activity of a manganese(II) isoindoline complex. J Inorg Biochem 102(4):773-780.

[42] Karipcin F, Uçan HI, Karataş I (2002) Binuclear and mononuclear cobalt(II), nickel(II) and copper(II) complexes of 4,4′-bis(alkylaminoisonitrosoacetyl)diphenyl-methane derivatives. Trans Met Chem 27:813-817.

[43] Karipcin F, Arabalı F, Karataş I (2006) Synthesis and characterization of 4-(alkylaminoisonitrosoacetyl)biphenyls and their complexes. Russ J Coord Chem 32:109-115.

[44] Ungnade HE, Fritz G, Kissinger LW (1963) Structure and physical properties of glyoximes. Tetrahedron 19:235-248.

[45] Ungnade HE, Kissinger LW, Narath A, Barham DC (1963) The structure of amidoximes. II.[1] Oxamidoxime. J Org Chem 28(1):134-136.

[46] Prushan MJ, Addison AW, Butcher RJ, Thompson LK (2005) Copper(II) complexes of tetradentate thioether-oxime ligands. Inorg Chim Acta 358:3449-3456.

[47] Kılıç A, Taş E, Gümgüm B, Yılmaz I (2006) Synthesis, spectral characterization and electrochemical properties of new vic-dioxime complexes bearing carboxylate. Trans Met Chem 31:645-652.

[48] Görgülü G, Çiçek MB, Dede B (2018) Synthesis and characterization of a novel aminoketooxime ligand and enzymatic efficiencies of its metal complexes, Acta Phys Pol A 133(2):244-249.

[49] Merrick JP, Moran D, Radom L (2007) An evaluation of harmonic vibrational frequency scale factors. J Phys Chem A 111(45):11683-11700.

[50] Gaber M, Ayad MM, El-Sayed YSY (2005) Synthesis, spectral and thermal studies of Co(II), Ni(II) and Cu(II) complexes 1-(4,6-dimethyl-pyrimidin-2-ylazo)-naphthalen-2-ol. Spectrochim Acta A 62:694-702.

[51] Shauib NM, Elassar AZA, El-Dissouky A (2006) Synthesis and spectroscopic characterization of copper(II) complexes with the polydentate chelating ligand 4,4'-[1,4-phenylenedi(nitrilo)dipente-2-one]. Spectrochim Acta A 63:714-722.

[52] Lever ABP (1997) Inorganic Electronic Spectroscopy, Elsevier, Amsterdam.

[53] Hathaway BJ (1987) Comprehensive Coordination Chemistry, Ed G. Wilkinson, R.D. Gillard, J.A. McCleverty, Pergamon Press, Oxford.

[54] Fukui K (1982) Role of frontier orbitals in chemical reactions. Science 218:747-754.

[55] Pearson RG (1986) Absolute electronegativity and hardness correlated with molecular orbital theory. Proc Natl Acad Sci 83(22):8440-8441.

[56] Ramalingam S, Karabacak M, Periandy S, Puviarasan N, Tanuja D (2012) Spectroscopic (infrared, Raman, UV and NMR) analysis, Gaussian hybrid computational investigation (MEP maps/HOMO and LUMO) on cyclohexanone oxime. Spectrochim Acta A 96:207-220.

[57] Suvitha A, Periandy S, Boomadevi S, Govindarajan M (2014) Vibrational frequency analysis, FT-IR, FT-Raman, ab initio, HF and DFT studies, NBO, HOMO-LUMO and electronic structure calculations on pycolinaldehyde oxime. Spectrochim Acta A 117:216-224.

[58] Neelakantan MA, Rusalraj F, Dharmaraja J, Johnsonraja S, Jeyakumar T, Pillai MS (2008) Spectral characterization, cyclic voltammetry, morphology, biological activities and DNA cleaving studies of amino acid Schiff base metal(II) complexes. Spectrochim Acta A 71(4):1599-1609.

[59] Sallam SA (2006) Binuclear copper(II), nickel(II) and cobalt(II) complexes with N_2O_2 chromophores of glycylglycine Schiff-bases of acetylacetone, benzoylacetone and thenoyltrifluoroacetone. Trans Met Chem 31(1):46-55.

[60] Xie H (2009) Aqua {4,4′-dibromo-6,6′-dimethoxy-2,2′-[ethane-1,2-diylbis(nitrilomethylidyne)]diphenolato} copper(II). Acta Crystallogr E: Struct Rep, 65(12):m1577-m1577.

[61] Geary WJ (1971) The use of conductivity measurements in organic solvents for the characterization of coordination compounds. Coordin Chem Rev 1(1):81-122.

[62] Anbu S, Kandaswamy M, Suthakaran P, Murugan V, Varghese B. (2009) Structural, magnetic, electrochemical, catalytic, DNA binding and cleavage studies of new macrocyclic binuclear copper (II) complexes. J Inorg Biochem 103(3):401-410.

[63] Rey NA, Neves A, Bortoluzzi AJ, Pich CT, Terenzi H (2007) Catalytic promiscuity in biomimetic systems: catecholase-like activity, phosphatase-like activity, and hydrolytic DNA cleavage promoted by a new dicopper(II) hydroxo-bridged complex. Inorg Chem, 46(2):348-350.

[64] Wolfe A, Shimer Jr GH, Meehan T (1987) Polycyclic aromatic hydrocarbons physically intercalate into duplex regions of denatured DNA. Biochemistry 26(20):6392-6396.

[65] El-Mehasseb IM, Ramadan AEMM, Issa RM (2006) Catecholase biomimetic catalytic activity of copper(II) complexes with 2-methyl-3-amino-(3H)-quinazolin-4-one. Trans Met Chem 31(6):730-739.

[66] Kovala-Demertzi D, Hadjikakou SK, Demertzis MA, Deligiannakis Y (1998) Metal ion-drug interactions. Preparation and properties of manganese(II), cobalt(II) and nickel(II) complexes of diclofenac with potentially interesting anti-inflammatory activity: Behavior in the oxidation of 3,5-di-*tert*-butyl-*o*-catechol. J Inorg Biochem 69(4):223-229.

Highlights

- Novel ligand and its Cu(II) and Mn(II) complexes were synthesized and characterized
- The quantum chemical calculations were performed by using DFT/B3LYP level of theory
- Inhibitory capacity of the ligand was investigated by molecular docking studies
- Complexes were tested for their catecholase and phenoxazinone synthase activity